

**NASA
Technical
Paper
3130**

1991

**Multidisciplinary Optimization
of Controlled Space Structures
With Global Sensitivity Equations**

Sharon L. Padula
*Langley Research Center
Hampton, Virginia*

Benjamin B. James
*Lockheed Engineering & Sciences Company
Hampton, Virginia*

Philip C. Graves
*ViGYAN, Inc.
Hampton, Virginia*

Stanley E. Woodard
*Langley Research Center
Hampton, Virginia*



National Aeronautics and
Space Administration
Office of Management
Scientific and Technical
Information Program

The use of trademarks or names of manufacturers in this report is for accurate reporting and does not constitute an official endorsement, either expressed or implied, of such products or manufacturers by the National Aeronautics and Space Administration.

Abstract

A new method for the preliminary design of controlled space structures is presented. The method coordinates standard finite-element structural analysis, multivariable controls, and nonlinear programming codes and allows simultaneous optimization of the structures and control systems of a spacecraft. Global sensitivity equations are a key feature of this method.

The preliminary design of a generic geostationary platform is used to demonstrate the multidisciplinary optimization method. Fifteen design variables are used to optimize truss-member sizes and feedback-gain values. The goal is to reduce the total mass of the structure and the vibration control system while satisfying constraints on vibration decay rate. Incorporating the nonnegligible mass of actuators causes an essential coupling between structural design variables and control design variables.

The solution of the demonstration problem is an important step toward a comprehensive controls-structures integrated design capability. Use of global sensitivity equations helps solve optimization problems that have a large number of design variables and a high degree of coupling between disciplines.

Introduction

Future NASA missions will include large space structures with control systems to damp out vibrations excited by pointing maneuvers. Preliminary design of these spacecraft is complicated by a high degree of coupling between the control and structural analyses. Specifically, changes in the structure impact the control system design by modifying both the plant to be controlled and the expected excitation. At the same time, changes in the control system impact the structural design by modifying the number, mass, and location of actuators. The preliminary design of controlled space structures is one aspect of a much broader program called the NASA Controls-Structures Interaction (CSI) Technology Program (ref. 1).

The CSI program encompasses a variety of research areas. The primary objectives of the program are (1) to develop analytical methods that characterize the performance of controlled space structures, (2) to develop controls-structures integrated design (CSID) methods, and (3) to improve ground test methods to better predict on-orbit system performance and validate the analytical methods. The first objective not only emphasizes the interaction between the structure and various control systems

but also quantifies the performance benefits and operational restrictions that result from this interaction (refs. 2 and 3). The second objective exploits advances in structural analysis, multivariable control, and multidisciplinary optimization for the preliminary design of large, flexible spacecraft (refs. 4 to 8). The third objective emphasizes hardware implementation and determines the validity of analytical assumptions. Thus, this objective requires new methods for accurate static and dynamic modeling of structural and control system hardware, innovative and physically realizable control strategies, and new methods for experimental system identification and verification (refs. 2, 3, and 9).

Research in CSID has grown during the past 10 years. Initial research studied the mechanisms that link structural characteristics to controlled performance by using simplified models and control theory. Reference 4 contains a survey of this work and concludes that strongly coupled CSID problems need attention. Recent research considered preliminary design problems that are complex enough to capture the most important characteristics of design problems associated with actual mission hardware. For example, researchers at NASA Langley Research Center have developed mathematical optimization procedures that successfully reduce surface distortion errors for large space antennas (ref. 5), tailor structures and control systems for reduced power consumption (ref. 6), and improve the fine-pointing performance of large space platforms while reducing mass (refs. 7 and 8).

The research reported in this paper addresses problems for which there is implicit coupling between structural design variables and control design variables. These optimization problems are challenging because they involve eigenvalue solvers and transient response analyses, which can be computationally expensive. Moreover, these analyses must be iterated until all structural and control response quantities converge.

The current research is unique because it coordinates commercial structural analysis codes, multivariable control codes, and optimization codes using the UNIX command language. This method can also be adapted for a variety of optimization problems associated with controlled space structures. The optimization method builds on recent advances in multidisciplinary analysis and optimization (refs. 10 to 12). Two key features of this research are the division of the system engineering problem into subproblems and the use of general-purpose analysis and optimization computer software for preliminary design studies. Because the disciplinary

analyses are tightly coupled, the global sensitivity equations (GSE) are used to calculate global derivatives of the response quantities with respect to the design variables. (See ref. 10.) For completeness, the GSE approach is compared with a more conventional approach.

The example used to illustrate the optimization method is the preliminary design of the structure and a vibration suppression controller for a geostationary platform subjected to slewing maneuvers. In this problem, truss-member sizes and controller gains are chosen to minimize spacecraft mass, which includes vibration control actuator mass. The mass of the vibration control actuators is a parameter that influences the spacecraft dynamic characteristics and a control system parameter that determines the maximum torque available for vibration suppression. Thus, the structural and control analyses are coupled by the presence of the nonnegligible actuator mass.

This paper develops and demonstrates a new technique for CSID. The design procedure is summarized, and alternative approaches for calculating global derivatives are discussed. The reference configuration and the optimization problem are presented with a brief discussion of the coupled disciplinary analyses. Typical results are presented, and a comparison between the GSE approach and a conventional approach is given.

Symbols and Abbreviations

CEC	collocated elastic control
CPU	central processing unit
CSI	controls-structures interaction
CSID	controls-structures integrated design
EAL	Engineering Analysis Language
$\mathbf{G}_p, \mathbf{G}_r$	position- and rate-gain matrices used to define collocated elastic control law
GSE	global sensitivity equations
\mathbf{g}	vector of 12 design variables used to define \mathbf{G}_p and \mathbf{G}_r matrices
I/O	input and output
\mathbf{J}	spacecraft inertia matrix, $\text{kg}\cdot\text{m}^2$
M_{act}	total mass of vibration suppression actuators, kg
M_s	total mass of truss structure, kg

n	number of modes used in reduced-order model of spacecraft
obj	objective function
\mathbf{r}	vector of three design variables used to define radii of truss-element cross section, m
\mathbf{v}	vector of design variable values associated with a specific stage in optimization procedure
x	arbitrary design variable, $x \in \{\mathbf{r}, \mathbf{g}\}$
y	arbitrary constraint function
α	distance between points in design space
δ	required vibration decay rate
λ	$2n \times 1$ vector of closed-loop eigenvalues, $\text{rad}^2/\text{sec}^2$
Φ	$3 \times n$ mode-slope matrix that contains rotational components of structural eigenvectors; superscript 0 indicates maneuver actuator location and superscripts 1 and 2 indicate first and second vibration-suppression-actuator locations
ω^2	$n \times 1$ vector of natural eigenvalues of the structural model, $\text{rad}^2/\text{sec}^2$

Multidisciplinary Optimization Procedure

CSID Method

There are three phases in the CSID process: analysis, calculation of global derivatives, and optimization. Analysis involves iteration between structural and control analyses until output quantities, such as structural mass and closed-loop response, converge. The global sensitivity calculation produces derivatives of response quantities for each design variable. The optimization phase searches for new values of design variables that reduce the objective function, reduce the degree of constraint violation, or both. Since the coupled analysis is expensive, linear approximations to the objective and constraint functions are used in the optimization phase. Limits on the allowable change in design variables restrict the search algorithm to a domain in which the linear approximations are appropriate. When no further reduction of the approximate objective function can be achieved without constraint violation, the coupled analysis and the global derivative calculations are repeated for the next set of design variables, and the

process continues. One repetition of analysis, derivative calculation, and optimization is referred to as one cycle. The CSID process continues until a prescribed maximum number of cycles is reached or until all constraints are satisfied and the change in the objective function is less than a prescribed convergence tolerance for two successive cycles.

A conventional three-phase CSID process is illustrated schematically in figure 1(a). The coupled analysis is represented by an iteration between the controls and structures computer codes. This coupled analysis is performed once at the nominal design point and is repeated after each design variable is perturbed. The global derivatives are approximated with a forward-difference formula. The optimization phase is represented by an iteration between the linear approximation and optimization computer codes. The linear approximation computer code calculates approximate values of both the objective function and the constraints by a first-order Taylor series extrapolation from the nominal solution by using gradient information provided by the global derivative phase. The optimization computer code is a general-purpose optimization program.

Figure 1(b) illustrates an alternative CSID approach in which the coupled analysis is used once per cycle. The controls and structures computer codes are modified to calculate the partial derivatives of output quantities with respect to input quantities. The global derivatives of response quantities with respect to each design variable are calculated with this local sensitivity derivative information.

The calculation of global derivatives in the alternative approach discussed in appendix A is implemented through the use of global sensitivity equations (GSE) described in references 10 and 13. The global derivatives are expressed as the solution to a set of linear equations whose coefficients are local sensitivity derivatives.

To calculate all global derivatives, it is necessary to solve a series of GSE problems that have the form

$$\begin{bmatrix} \mathbf{I} & -\frac{\partial \mathbf{C}}{\partial \mathbf{S}} \\ -\frac{\partial \mathbf{S}}{\partial \mathbf{C}} & \mathbf{I} \end{bmatrix} \begin{Bmatrix} \frac{d\mathbf{C}}{dx} \\ \frac{d\mathbf{S}}{dx} \end{Bmatrix} = \begin{Bmatrix} \frac{\partial \mathbf{C}}{\partial x} \\ \frac{\partial \mathbf{S}}{\partial x} \end{Bmatrix} \quad (1)$$

where \mathbf{I} is the identity matrix, \mathbf{S} is the set of all structural outputs, \mathbf{C} is the set of all control outputs, and x is any global design variable. Standard mathematical computer software can be used to solve equation (1) for each design variable x . The multiple solutions are calculated efficiently since only the right-hand side changes.

In this paper, both the conventional and the GSE approach are used. The conventional approach is recommended for uncoupled problems. In this case, the disciplinary analyses can be computed without iteration, and finite-difference approximations to global derivatives are tractable. The conventional approach is also recommended for coupled problems for which the number of structural modes used in the control analysis is large compared with the number of design variables. In this case, the dimensions of the GSE matrix can become large, and the cost of evaluating the local derivatives can become excessive. On the other hand, the GSE approach is ideal when the number of design variables is so large that repeated perturbations of the coupled analysis is computationally prohibitive. The size of the GSE matrix is unaffected by the number of design variables x . Increasing the number of design variables means that equation (1) must be solved for additional right-hand sides. This impacts the computational cost only when the local derivatives in the added column vectors are expensive to calculate.

Demonstration Problem

The preliminary design of a generic geostationary platform is used to develop and demonstrate the CSID methods. The goal is to reduce the total mass of the structure and the vibration control system while satisfying constraints on vibration decay rate. Standard finite-element analysis, multivariable control, and mathematical programming routines are coordinated by a new multidisciplinary optimization scheme.

The reference configuration, shown in figure 2, represents a large geostationary platform, which consists of two antennas connected by a bus structure. The platform has three sets of actuators; each set supplies three-axis torques. Two of the actuator sets work together for vibration suppression control. These sets are mounted at the intersection of the centerline of the bus structure and the axis of symmetry of each antenna. The third set of actuators is used to perform rigid-body rotational maneuvers and is located at an arbitrary joint in the bus structure near the center of mass. A finite-element model is assembled from beam elements to represent a graphite-epoxy truss structure. Three groups of beam elements are defined: the bus, the antennas, and the antenna supports. All beam elements have the same wall thickness, but the outer radius may vary from one group of elements to another.

To obtain a tractable integrated design problem, certain simplifying assumptions are made. The locations of the three actuator sets are fixed, the mass

of the maneuver actuator is ignored, and the inertia matrix \mathbf{J} is calculated at the fixed maneuver location rather than at the variable center-of-mass location. Vibration-suppression-actuator masses are included in the model, but their rotational inertias are not included. The masses of scientific payloads, power-generating and power-distribution hardware, computers, and other supporting equipment are ignored. The mass and dynamic characteristics of the joints between truss elements are also neglected. The stiffness contribution of the surface material of the antenna reflector is neglected, but the mass is modeled approximately. Minimum gage constraints on the truss-member sizes are also used instead of stress and buckling constraints. The structural model is discussed in appendix B.

To complete the structural model, the masses of the two vibration suppression actuators must be determined and incorporated into the model. A constraint in the control law design requires that the vibration suppression actuators to have the same mass. To determine the actuator mass, first a torque history characteristic of a minimum-time rigid-body rotational maneuver is applied to the elastic spacecraft with the vibration suppression loop closed. The mass of each actuator is calculated based on the sum of the maximum torques about each axis required to suppress vibrations that occur after this reference maneuver. The total mass is obtained by multiplying the number of actuators (two) by the mass per actuator. The actuator mass calculation is discussed in appendix C.

Controls-structures integrated design of the reference configuration is implemented with a mathematical programming method used to adjust the values of 15 design variables. Three design variables r_i control the outer cross-sectional radius of the groups of beam elements that comprise the bus structure ($i = 1$), the antennas ($i = 2$), and the antenna supports ($i = 3$). The remaining 12 design variables g_i ($i = 1, 2, \dots, 12$) uniquely determine the elements of the position- and rate-gain matrices for the vibration control system.

The optimization problem is to minimize the total mass of the platform while satisfying vibration decay requirements. This problem can be stated in terms of the total mass of the truss structure M_s , the total mass of the vibration suppression actuators M_{act} , and the complex-valued, closed-loop eigenvalues λ_i . Minimize

$$M_s + M_{act} \quad (2a)$$

subject to

$$\text{Re}(\lambda_i) \leq \delta \quad (i = 1, 2, \dots, 2n) \quad (2b)$$

where δ is the required decay rate and n is the number of modes used in the reduced-order model of the spacecraft. The calculation of the real part of the closed-loop eigenvalues is discussed in appendix C. In the remainder of the paper, λ_i is used to stand for $\text{Re}(\lambda_i)$.

This design problem is particularly challenging because the structural and control analyses are tightly coupled. Changes to the structural design variables (truss sizes) change the open-loop plant and thus the closed-loop response to the reference maneuver. On the other hand, changes to the control design variables (the gains) determine the vibration-suppression-actuator torques, which are linearly related to the actuator masses used in the structural model.

Controls-Structures Analyses

This section briefly describes the structural and control analyses and explains the successive substitution algorithm used to solve the coupled problem. The inputs to the coupled controls-structures analyses are the design variables, and the outputs are M_s , M_{act} , and λ used in equations (2).

The structural analysis consists of finite-element analysis of the spacecraft structure through the use of the Engineering Analysis Language (EAL) computer code. (See ref. 14.) The mass and stiffness matrices are assembled based on the current values of the design variables r_i and the mass of the actuators M_{act} . A real symmetric eigenvalue problem is solved to obtain the characteristic modes and frequencies of the truss structure. Outputs from the structural analysis include the first n eigenvalues ω^2 and the first n mode slopes (i.e., rotational components of the eigenvectors) at the maneuver actuator location $\Phi^{(0)}$ and at the vibration-suppression-actuator locations $\Phi^{(1)}$ and $\Phi^{(2)}$. In addition, the mass of the bare structure M_s and the inertia matrix \mathbf{J} associated with the maneuver actuator location are output. All these outputs, except for M_s , are inputs to the control analysis.

The control analysis determines the transient closed-loop response of the spacecraft to a reference maneuver and searches for the maximum vibration control torques and the times at which they occur. The maneuver is assumed to be linear since it rotates the spacecraft through small angles during a long period of time. Thus, the nonlinear coupling of rigid and elastic motion that is typical of rotational maneuvers is not modeled. The maneuver represents a typical disturbance that might be encountered by the geostationary platform. The vibration suppression

system employs collocated elastic control (CEC) with a single pair of actuators constrained so that their net torque output is zero. The robust dissipative control law used by CEC does not affect rigid-body motion and guarantees stability despite unmodeled dynamics and parameter uncertainty (refs. 15 to 17). The torque required by the CEC actuators is a function of the angular deformations and angular deformation rates at the actuator locations and the values of the 12 design variables g_j , which uniquely determine the position-gain matrix \mathbf{G}_p and rate-gain matrix \mathbf{G}_r . The complete control analysis is contained in appendix C.

The actuators are sized based on the peak torques required to suppress the elastic motion that remains after the reference maneuver. The mass of actuators needed to provide the peak torques can be interpolated from an empirical table of mass versus torque for available actuators. For the present study, however, a linear relationship between actuator mass and maximum torque output is assumed. Outputs from the control analysis include M_{act} and the $2n$ complex closed-loop eigenvalues λ . The actuator mass M_{act} is an input to the structural analysis.

The solution to the coupled controls-structures analysis problem is found by iteration. Figure 3 shows a flow chart of the iterative procedure that starts with an initial estimate of the actuator mass. This value of M_{act} is incorporated into the structural model. The required actuator mass is determined from the transient response calculated in the control analysis. If the value of M_{act} used in the structural model and the value calculated by the control analysis are within 1 percent of each other, then the procedure terminates. Otherwise, the required actuator mass is used in the structural analysis (i.e., the mass matrix is updated) and the iteration continues.

The above procedure was modified to improve efficiency. The computational cost of the procedure is dominated by the cost of solving the structural eigenvalue problem. Fortunately, calculating the sensitivity of the solution of the eigenvalue problem to changes in lumped masses (e.g., $\partial\omega^2/\partial M_{\text{act}}$) is relatively inexpensive. (See refs. 18 and 19.) Therefore, the change in structural outputs with a change in M_{act} can be estimated when the change is sufficiently small. Currently, the full structural analysis is repeated only when the change in actuator mass exceeds 10 percent of the initial estimate. Otherwise, the structural outputs are estimated from sensitivity information.

The modification for efficiency required one additional change in the procedure. If the change in M_{act} is less than 1 percent but is based on an estimate of the structural outputs, then one additional execution of the structural and control analyses is needed to confirm convergence. During the additional execution of the structural analysis, the local derivatives (e.g., $\partial\omega^2/\partial r_2$) of structural outputs with respect to design variables are calculated, along with the local derivatives with respect to M_{act} .

GSE and Optimization

This section contains a summary of the global derivative calculation and the optimization process required to complete one cycle of the new CSID procedure. These calculations, which take place after the controls-structures analysis has converged, assume that values of the output quantities \mathbf{J} , ω , $\Phi^{(0)}$, $\Phi^{(1)}$, $\Phi^{(2)}$, M_s , M_{act} , and λ are available.

To solve the GSE problem (eq. (1)), all local derivatives that are the coefficients of the matrix equations must be evaluated. That is, for each contributing analysis, the partial derivatives of each output quantity with respect to each input quantity must be calculated or estimated. For the demonstration problem, the contributing analyses are controls and structures, and the input and output quantities are shown in figure 4. All partial derivatives are scaled according to the scheme suggested in reference 20 and placed in the GSE as discussed in appendix A.

The set of linear GSE (eq. (1)) is assembled and solved to determine the global derivatives of M_s , M_{act} , and λ with respect to each design variable. For example, one of these linear equations is

$$\begin{aligned} \frac{dM_{\text{act}}}{dr_2} = & \sum_{i=1}^n \frac{\partial M_{\text{act}}}{\partial \omega_i} \frac{d\omega_i}{dr_2} \\ & + \sum_{i=1}^6 \frac{\partial M_{\text{act}}}{\partial J_i} \frac{dJ_i}{dr_2} \\ & + \sum_{i=1}^{3n} \sum_{j=0}^2 \frac{\partial M_{\text{act}}}{\partial \phi_i^{(j)}} \frac{d\phi_i^{(j)}}{dr_2} \end{aligned} \quad (3)$$

Equation (3) reflects the fact that the required actuator mass is not influenced directly by the truss sizing variable r_2 (i.e., $\partial M_{\text{act}}/\partial r_2 = 0$) but is influenced indirectly by the eigenvalues and the elements of the inertia and mode-slope matrices. The notation d/dr_2 signifies the global derivative with respect to r_2 . Thus, the global derivatives quantify the effect

of coupling between the local control and structural analyses.

Once the global derivatives are available, they can be used to provide linear approximations to the objective function and the normalized constraint function y_i . For example, given

$$\left. \begin{aligned} \text{obj} &= M_s + M_{\text{act}} \\ y_i &= 1 - \frac{\lambda_i}{\delta} \quad (i = 1, 2, \dots, 2n) \end{aligned} \right\} \quad (4)$$

where $y_i \leq 0$ is a feasible constraint, and the required decay rate δ is a negative real number; therefore, the effect of changing an arbitrary design variable x by the amount Δx is approximated by

$$\left. \begin{aligned} \text{obj}(x + \Delta x) &\approx M_s + \frac{dM_s}{dx} \Delta x \\ &\quad + M_{\text{act}} + \frac{dM_{\text{act}}}{dx} \Delta x \\ y_i(x + \Delta x) &\approx 1 - \frac{\lambda_i}{\delta} - \frac{d\lambda}{dx} \frac{\Delta x}{\delta} \end{aligned} \right\} \quad (5)$$

The solution of the optimization problem in equations (2) is accomplished by linking the linear approximation routine with the standard nonlinear programming code CONMIN (ref. 21). A nonlinear programming code was selected because future CSID projects may require nonlinear objective and constraint functions.

Results and Discussion

Demonstration Overview

All results in this section were generated with the GSE approach. The impact of choosing the GSE approach over the conventional approach is discussed in the section "Comparison of GSE and Conventional Approach." The implementation details are discussed in appendix D.

The proper operation of the optimization procedure is demonstrated through convergence to the same solution from two different initial design points. In each case, the total mass of the reference configuration is minimized with respect to 15 design variables (eqs. (2)). The decay rate requirement is $\delta = -0.03$. The reference maneuver rotates the spacecraft 20° about all axes simultaneously in 10 sec. Limits are set so that a design variable may change no more than 10 percent during a single cycle. The number of modes and frequencies that describe the open-loop model was $n = 20$, and 0.5 percent modal damping was assumed.

Case 1: slightly infeasible initial design.

Demonstration case 1 has an initial design that does not fulfill the decay rate requirement. The initial values of the truss sizing variables are $r_1 = 4$, $r_2 = 4$, and $r_3 = 8$ cm. These sizes yield an initial structural mass of 1158 kg. The frequencies of the first five elastic modes are 0.668, 0.977, 1.35, 1.48, and 1.48 Hz. The fourth and fifth vibrational frequencies are identical (i.e., they are repeated eigenvalues) because of structural symmetries in the spacecraft antennas. Both closely spaced and repeated frequencies are characteristic features of large space structures and are considered in this demonstration problem. The initial values of the position- and rate-gain matrices are

$$\mathbf{G}_p = \mathbf{G}_r = \begin{bmatrix} 5100 & 800 & 700 \\ 800 & 5000 & 700 \\ 700 & 700 & 4900 \end{bmatrix} \quad (6)$$

The closed-loop response that results from these gains indicates an actuator mass requirement of only 10.69 kg. The first five closed-loop eigenvalue pairs are $-0.021 \pm 4.2j$, $-0.031 \pm 6.1j$, $-0.049 \pm 8.5j$, $-0.047 \pm 9.3j$, and $-0.047 \pm 9.3j$. Only the first pair violates the constraint that $\text{Re}(\lambda) \leq -0.03$.

Figure 5 contains optimization histories for demonstration case 1. Figure 5(a) shows the history of the objective (i.e., total mass) with respect to the optimization cycle. The CSID procedure increases the total mass during the first five cycles and decreases the total mass at each cycle thereafter. The initial increase in total mass is associated with a rapid decrease in the constraint violation, as indicated in figure 5(b). This figure shows that the maximum eigenvalue constraint $\max[\text{Re}(\lambda)]$ decreases smoothly to the constraint boundary in five cycles. The maximum constraint value oscillates around the constraint boundary beginning at cycle 15. Such behavior is common when a linear approximation to nonlinear constraints is used.

Figures 5(c) to 5(e) contain histories of selected design variable values. Only the diagonal elements of the gain matrices \mathbf{G}_p and \mathbf{G}_r are plotted. The off-diagonal elements never change significantly from their initial values. A comparison of these histories with those in figure 5(a) shows that the initial increase in total mass is associated with increases in all three structural design variables and in rate gain. The subsequent decrease in mass is associated with a decrease in the radii of the bus truss. A decrease in rate gain also contributes, but this decrease lags the structural changes. This effect implies that changes in the structure not only decrease mass but also

reduce the amount of control effort required to meet decay rate constraints.

Figure 5(f) is similar to figure 5(a) but uses a different scale for the actuator mass. This figure indicates that the actuator mass requirements are changed by ± 25 percent from cycle to cycle, even when the change in design variables is much smaller. This behavior emphasizes that the amount of control effort required is a function of diverse factors, such as dynamic and inertial properties of the structure plus adjustments to the control system. More importantly, figure 5(f) indicates that an increase in actuator mass from about 10 to 50 kg allows a reduction of about 300 kg in total mass. This favorable trade-off of structure mass for control effort is the major benefit of an integrated controls-structures optimization procedure.

Case 2: highly infeasible initial design.

Demonstration case 2 has an initial design that has a smaller total mass and a greater constraint violation than the first case. The only difference between the cases is that initial values of the truss sizing variables are each set to 2 cm. This causes the first seven pairs of closed-loop eigenvalues to violate the decay rate constraint. Figure 6 contains a convergence history of mass with respect to optimization cycle. This second case converges to the same total mass as the first case, namely, about 850 kg with an actuator mass of about 50 kg.

One way to compare the optimization histories of the two cases is to plot the maximum eigenvalue constraint versus total mass. (See fig. 7.) In this figure, movement downward and to the left signifies improvement of the design from one cycle to the next. The two demonstration problems start at different initial conditions and follow different convergence paths. However, the final conditions are similar. This similarity shows that the optimization procedure performs well (consistently produces an improved design) and that the final solution is possibly a global minimum.

Although the optimization procedure converges to equally satisfactory solutions from different initial design points, the convergence path of demonstration case 1 is less direct than that of case 2. The path of case 2 makes consistent progress toward the final solution, while the path of case 1 initially adds an unnecessary amount of mass. Two of the structural design variables increase during the early optimization cycles but return to their initial values at the end of the optimization process. (See fig. 5(c).) This observation, and the previously noted oscillation of the maximum constraint value around the constraint

boundary, suggests that the quality of global derivatives should be investigated. The derivatives may be accurate, but the move limits allow design variable values to change so much that the linear approximation is a poor representation of the coupled analysis. Alternately, the global derivatives calculated by the GSE approach may be deficient.

A simple test can be used to determine the quality of global derivatives that were calculated in demonstration case 1. Two design points \mathbf{v}_1 and \mathbf{v}_2 that correspond to successive optimization cycles are selected. A coupled analysis is performed at each design point and at evenly spaced intermediate points so that:

$$\mathbf{v}_{\text{new}} = \alpha \mathbf{v}_2 + (1 - \alpha) \mathbf{v}_1 \quad (\alpha = 0, 0.1, \dots, 1.0) \quad (7)$$

where \mathbf{v}_{new} is a sequence of intermediate points between the chosen design points \mathbf{v}_1 and \mathbf{v}_2 . Figure 8(a) compares the actuator mass calculated by the coupled analysis with the mass predicted with nominal values and global derivatives at the point \mathbf{v}_1 . In this case, \mathbf{v}_1 and \mathbf{v}_2 are the design points associated with cycles 18 and 19 in figure 5. The difference between actual and approximate M_{act} is small at $\alpha = 0.1$, but this difference is large at $\alpha = 1.0$. This change indicates that the global derivatives are calculated correctly but that the move limits need to be small if the linear approximations for actuator mass are to remain valid. Fortunately, this discrepancy is less severe for the prediction of closed-loop eigenvalues. Figure 8(b) contains the corresponding comparison of the real part of the maximum eigenvalue with the linear approximation to this value. The behavior is more nearly linear, and the error caused by the current move limits is acceptable.

Assessment of GSE Approach

This paper investigates the use of the GSE approach to provide global derivatives for CSI optimization problems. As previously discussed, the GSE approach provides high-quality derivative information. In this section, the strengths and weaknesses of GSE are discussed from an implementation standpoint. The strengths involve numerical, efficiency, human judgment, and organizational issues; the weaknesses include implementation complexity and computer memory requirements.

The numerical argument for the GSE approach is that it is relatively insensitive to the degree of convergence of the iterative (coupled) analysis. The iterative procedure (fig. 3) terminates based on the percentage change in the mass of actuators. The current study experimented with 1 and 0.1 percent

convergence criteria for the iterative analysis and found little difference in the optimization results. On the other hand, 0.05 percent was the *largest* convergence criterion that produced acceptable results when global derivatives were estimated by the conventional approach (finite differencing over the coupled analysis). A small convergence criterion means many additional iterations of the coupled analysis and additional computational expense.

For CSID problems, the GSE approach is efficient. The coupled analysis is performed only once per cycle; thus, the number of structural eigenvalue problems to be solved is kept to a minimum. The structural code is computationally expensive and requires large amounts of computer memory. For instance, in the demonstration problem, the finite-element analysis required 20 times more central processing time and 20 times more disk space than the control analysis required. The GSE approach requires the calculation of many additional local derivatives, but most of these calculations involve reduced-order control analysis.

Another strong argument for the GSE approach involves human judgment. As a rule, researchers lack confidence in global derivatives of a multidisciplinary analysis whether the derivatives are calculated by the conventional approach or by the GSE approach. On the other hand, individual entries in the GSE matrix (which result from local analyses) generally have physical meaning. For example, numerical values that indicate the dependence of closed-loop eigenvalues on open-loop frequencies, or the dependence of the inertia properties of the structure on actuator mass, may have intuitive appeal. These physically meaningful quantities are often available as an output option from the standard analysis codes. For instance, semianalytic formulas for structural derivatives are common. (See appendix B.) When this is not true, the local derivatives can be estimated by finite-difference approximation. Finite-difference approximations to the control derivatives proved to be accurate. (See appendix C.)

A final argument for GSE, which is mentioned in reference 10, is realized in the current research. The GSE approach facilitates the smooth operation of a multidisciplinary design team. In the current research, some team members had more experience with control theory, and others had more experience with structural analysis. Members used their own expertise to develop the local analysis and local derivative capabilities. Once individual codes were operational, they were combined with generic global sensitivity and optimization routines. The end

result was a powerful and flexible CSI optimization capability.

Complexity is one definite disadvantage of the GSE approach. A large number of local derivatives must be communicated to the GSE computer code in exactly the correct form and order. Inconsistencies within the coupled analysis can be a problem. For instance, the structural outputs contain derivatives of ω^2 , but the control analysis calculates derivatives with respect to ω .

Another potential disadvantage of the GSE approach is the size of the set of linear equations to be solved. For the current example, the size never exceeded 228×228 and thus was not a concern. The number 228 represents 2 masses, 6 unique components of the symmetric inertia matrix, 180 elements of the 3 mode-slope matrices, 20 elastic modal frequencies, and 20 unique real parts of the closed-loop eigenvalues. The actual size is slightly smaller because repeated eigenvalues (due to structural symmetry) are eliminated. The size of the GSE matrix can expand if the number of modes used in the reduced-order model increased or if additional constraints (e.g., structural member buckling constraints) are added to the optimization problem.

Comparison of GSE and Conventional Approaches

In the final analysis, the value of the GSE approach needs to be assessed relative to the conventional approach. Clearly, it is easier to develop a procedure that perturbs the coupled analysis many times and estimates the global derivatives through the use of a forward-difference formula than it is to calculate and manipulate the local derivatives and solve equation (1). However, choosing a perturbation step size is difficult. The accepted method for choosing step size is to test successively smaller steps and stop when no significant change in output occurs. This method assumes that the coupled analysis is perfectly converged; thus, the method requires many repetitions of controls and structures codes to satisfy a small convergence tolerance. As a consequence, this method of determining step size is expensive. Moreover, the step size that proves to be appropriate for a given design point is not guaranteed to remain appropriate throughout the problem domain.

To compare the GSE and conventional approaches, demonstration case 1 was solved by each method. As shown in figure 9, the two approaches have similar convergence histories. The computational cost per cycle for 15 design variables and 20 modes is about the same. The perturbation step size for the

conventional approach was set at 0.01 percent of the nominal value of each design variable.

Choosing the proper step size for the conventional approach was difficult. Perturbation step sizes that were several orders of magnitude larger and smaller than 0.01 percent were investigated at the initial design point. Each of the three structural design variables was perturbed separately. The global derivatives varied enormously with the perturbation step size (i.e., changes in sign and in order of magnitude were observed), and the choice of appropriate step size was not clear. Eventually, the perturbation step size was chosen by comparison of the finite-difference derivatives with the global derivatives calculated by the GSE approach. This experience suggests that the GSE approach is the best choice when the control and structural analyses are tightly coupled, that is, when an iteration between the analyses is required for solution.

In summary, the GSE approach should be favored for problems with a large number of design variables and for problems in which the coupling between disciplines is strong. When a large number of design variables occur, the GSE approach is more efficient, and when coupling between disciplines is strong, the GSE approach is not sensitive to poor choices of convergence tolerance or perturbation step size.

Concluding Remarks

This paper describes the development and implementation of a general optimization-based method for the design of large space platforms through integration of the disciplines of structural dynamics and controls. The method is especially appropriate for preliminary design problems in which the structural and control analyses are tightly coupled. The method

is significant because it coordinates general-purpose structural analysis, multivariable control, and optimization codes and thus can be adapted to a variety of controls-structures integrated design (CSID) projects. The method uses the global sensitivity equations (GSE) approach. Although the GSE approach has been applied to other preliminary design problems, this is the first application to the design of a large space structure.

To demonstrate its capabilities the method is used to minimize the total weight of a space platform while maintaining a specified vibration decay rate after slewing maneuvers. Although the structural model has many simplifying assumptions and the number and location of actuators are fixed, this proves to be a challenging design problem. With the CSID procedure, the platform is redesigned so that the mass distribution and dynamic characteristics of the structure enhance the use of rate and position feedback by the control system. The CSID method must trade stiffness that adds structural weight for control effort that adds weight to the actuators. The procedure not only makes a favorable trade of structural mass for control effort but also satisfies the vibration decay rate constraints.

This research demonstrates that an integrated controls-structures optimization method can lead to significant mass savings, which may not be revealed by traditional (single-discipline) design methods. The solution of the demonstration problem is an important step toward comprehensive preliminary design capability for controlled space structures.

NASA Langley Research Center
Hampton, VA 23665-5225
September 27, 1991

Appendix A

Global Sensitivity Equations

This appendix describes the use of global sensitivity equations (GSE) to calculate derivatives of integrated controls-structures response quantities with respect to design variables and emphasizes the application of GSE to the demonstration problem. References 10 to 12 discuss the theoretical foundations and other applications of GSE.

In theory, the GSE approach can be applied to coupled problems with any number of contributing analyses. The global derivatives are determined by solution of a set of linear equations of the form

$$\mathbf{A}\mathbf{h} = \mathbf{B} \quad (\text{A1})$$

where \mathbf{A} is a matrix of coefficients, \mathbf{h} is the solution vector, and \mathbf{B} is a matrix of one or more right-hand-side column vectors.

The size and topology of the GSE are determined by the application. For the demonstration problem (eqs. (2)), there are two contributing analyses: controls and structures. The inputs and outputs of these analyses are shown in figure 4. There are 15 design variables \mathbf{r} and \mathbf{g} and thus 15 column vectors in the matrix \mathbf{B} . There are 42 response quantities M_s , M_{act} , and λ and 206 outputs of the structural analysis that influence the control analysis (ω , $\Phi^{(0)}$, $\Phi^{(1)}$, $\Phi^{(2)}$, and \mathbf{J}). The preceding counts assume that $n = 20$. Thus, matrix \mathbf{A} in equation (A1) has at most 248×248 entries.

The actual number of coefficients that need to be computed is smaller than the maximum number of entries in matrix \mathbf{A} . The closed-loop eigenvalues λ occur in conjugate pairs, and only the real part of each complex number is constrained. Generally, no more than 20 of the 40 closed-loop eigenvalues have unique values or unique partial derivatives. Likewise, the open-loop eigenvalues ω^2 are not all unique. Because of the symmetry of the structure, some eigenvalues are paired. Furthermore, since none of the design variables or response quantities alter the symmetry of the structure, the partial derivatives of eigenvalues with respect to changes in the input quantities also occur in pairs. Removing from matrix \mathbf{A} rows and columns that correspond to nonunique quantities gives a matrix with about 220×220 elements. The exact number can change depending upon which structural modes are retained in the reduced model. Many of these elements have the value of zero and do not need to be computed.

The topology of matrix \mathbf{A} for the reference problem is

$$\mathbf{A} = \begin{bmatrix} \mathbf{I}_{(22 \times 22)} & \mathbf{A}_2_{(22 \times 198)} \\ \mathbf{A}_1_{(198 \times 1)} & \mathbf{0}_{(198 \times 21)} \quad \mathbf{I}_{(198 \times 198)} \end{bmatrix} \quad (\text{A2})$$

where the submatrices have the indicated sizes and \mathbf{I} is the identity matrix, $\mathbf{0}$ indicates a submatrix filled with zeros, and submatrix \mathbf{A}_1 is defined as

$$\mathbf{A}_1^T = \left[-\frac{\partial \omega_1}{\partial M_{\text{act}}}, \dots, -\frac{\partial \omega_n}{\partial M_{\text{act}}}, -\frac{\partial \phi_{11}^{(1)}}{\partial M_{\text{act}}}, \dots, -\frac{\partial \phi_{3n}^{(3)}}{\partial M_{\text{act}}}, -\frac{\partial J_1}{\partial M_{\text{act}}}, \dots, -\frac{\partial J_6}{\partial M_{\text{act}}} \right] \quad (\text{A3})$$

where the local derivatives are calculated by a semianalytic method discussed in appendix B. The submatrix \mathbf{A}_2 is defined as

$$\mathbf{A}_2 = \begin{bmatrix} -\frac{\partial M_{\text{act}}}{\partial \omega_1} & \dots & -\frac{\partial M_{\text{act}}}{\partial \omega_n} & -\frac{\partial M_{\text{act}}}{\partial \phi_{11}^{(1)}} & \dots & -\frac{\partial M_{\text{act}}}{\partial \phi_{3n}^{(3)}} & -\frac{\partial M_{\text{act}}}{\partial J_1} & \dots & -\frac{\partial M_{\text{act}}}{\partial J_6} \\ -\frac{\partial \lambda_1}{\partial \omega_1} & \dots & -\frac{\partial \lambda_1}{\partial \omega_n} & -\frac{\partial \lambda_1}{\partial \phi_{11}^{(1)}} & \dots & -\frac{\partial \lambda_1}{\partial \phi_{3n}^{(3)}} & -\frac{\partial \lambda_1}{\partial J_1} & \dots & -\frac{\partial \lambda_1}{\partial J_6} \\ \vdots & \ddots & \vdots & \vdots & \ddots & \vdots & \vdots & \ddots & \vdots \\ -\frac{\partial \lambda_n}{\partial \omega_1} & \dots & -\frac{\partial \lambda_n}{\partial \omega_n} & -\frac{\partial \lambda_n}{\partial \phi_{11}^{(1)}} & \dots & -\frac{\partial \lambda_n}{\partial \phi_{3n}^{(3)}} & -\frac{\partial \lambda_n}{\partial J_1} & \dots & -\frac{\partial \lambda_n}{\partial J_6} \\ 0 & \dots & 0 & 0 & \dots & 0 & 0 & \dots & 0 \end{bmatrix} \quad (\text{A4})$$

where all local derivatives are approximated by finite differencing.

Matrix \mathbf{B} in equation (A1) has rows that are associated with each unique response quantity and each unique output of the structural analysis and are ordered to be consistent with matrix \mathbf{A} ; the columns in matrix \mathbf{B} correspond to the design variables. Thus, matrix \mathbf{B} has the form

$$\mathbf{B} = \begin{bmatrix} \mathbf{0}_{(21 \times 3)} & \mathbf{B}_{2(21 \times 12)} \\ \mathbf{B}_1_{(199 \times 3)} & \mathbf{0}_{(199 \times 12)} \end{bmatrix} \quad (\text{A5})$$

where

$$\mathbf{B}_1 = \begin{bmatrix} \frac{\partial M_s}{\partial r_1} & \frac{\partial M_s}{\partial r_2} & \frac{\partial M_s}{\partial r_3} \\ \frac{\partial \omega_1}{\partial r_1} & \frac{\partial \omega_1}{\partial r_2} & \frac{\partial \omega_1}{\partial r_3} \\ \vdots & \vdots & \vdots \\ \frac{\partial \omega_n}{\partial r_1} & \frac{\partial \omega_n}{\partial r_2} & \frac{\partial \omega_n}{\partial r_3} \\ \frac{\partial \phi_{11}^{(1)}}{\partial r_1} & \frac{\partial \phi_{11}^{(1)}}{\partial r_2} & \frac{\partial \phi_{11}^{(1)}}{\partial r_3} \\ \vdots & \vdots & \vdots \\ \frac{\partial \phi_{3n}^{(3)}}{\partial r_1} & \frac{\partial \phi_{3n}^{(3)}}{\partial r_2} & \frac{\partial \phi_{3n}^{(3)}}{\partial r_3} \\ \frac{\partial J_1}{\partial r_1} & \frac{\partial J_1}{\partial r_2} & \frac{\partial J_1}{\partial r_3} \\ \vdots & \vdots & \vdots \\ \frac{\partial J_6}{\partial r_1} & \frac{\partial J_6}{\partial r_2} & \frac{\partial J_6}{\partial r_3} \end{bmatrix} \quad (\text{A6})$$

and

$$\mathbf{B}_2 = \begin{bmatrix} \frac{\partial M_{\text{act}}}{\partial q_1} & \cdots & \frac{\partial M_{\text{act}}}{\partial q_{12}} \\ \frac{\partial \lambda_1}{\partial q_1} & \cdots & \frac{\partial \lambda_1}{\partial q_{12}} \\ \vdots & \ddots & \vdots \\ \frac{\partial \lambda_n}{\partial q_1} & \cdots & \frac{\partial \lambda_n}{\partial q_{12}} \end{bmatrix} \quad (\text{A7})$$

As with the \mathbf{A} submatrices, the components of \mathbf{B}_1 are evaluated with semianalytic formulas, and the components of \mathbf{B}_2 are evaluated with finite differences.

The solution vector \mathbf{h} in equation (A1) contains global derivatives of response and structural output quantities with respect to each of the 15 design variables. Thus, for the first design variable (which corresponds to the first column vector in matrix \mathbf{B})

$$\mathbf{h}_1^T = \left[\frac{dM_{\text{act}}}{dr_1}, \frac{d\lambda_1}{dr_1}, \dots, \frac{d\lambda_n}{dr_1}, \frac{dM_s}{dr_1}, \frac{d\omega_1}{dr_1}, \dots, \frac{d\omega_n}{dr_1}, \frac{d\phi_{11}^{(1)}}{dr_1}, \dots, \frac{d\phi_{3n}^{(3)}}{dr_1}, \frac{dJ_1}{dr_1}, \dots, \frac{dJ_6}{dr_1} \right] \quad (\text{A8})$$

The first $2 + n$ entries in each \mathbf{h}_i vector contain global derivatives that are needed by the optimization phase of the controls-structures integrated design (CSID) process.

The solution of equation (A1) is calculated with a standard lower and upper triangular decomposition algorithm. The computer code that solves equation (A1) also estimates the condition number N of the matrix defined as

$$N = \|\mathbf{A}\| \|\mathbf{A}^{-1}\| \quad (\text{A9})$$

where the matrix norm is defined as

$$\|\mathbf{A}\| = \max_j \left(\sum_i |a_{ij}| \right) \quad (\text{A10})$$

Condition numbers between 10^3 and 10^6 were typical for the demonstration problems. These exponents suggest a loss of 3 to 6 significant figures (out of about 14 significant figures on a 64-bit machine) due to numerical errors during the solution of equation (A1). The effect of conditioning errors would have been greater than this if the individual entries in the GSE matrix were not scaled as suggested in reference 20. For example, $\partial M_{\text{act}}/\partial J_3$ is multiplied by J_3/M_{act} before being placed in the GSE matrix. After equation (A1) is solved, the true values of the global derivatives can be recovered through reversal of the scaling procedure.

Appendix B

Structural Analysis

This appendix describes the structural model used in the demonstration problems. The definitions of the structural design variables are given, and the procedures used to calculate the outputs of the structural analysis are explained. The finite-element model, comprised of beam elements and point masses, is assembled with the program Engineering Analysis Language (EAL; see ref. 14).

The geometry of the reference configuration is shown in figure 2. The size and shape of the platform does not change during the optimization process. Structural elements are divided into three groups (bus, antenna, and antenna support) and are sized by the optimization process. The three design variables r_i control the outer radius of groups of structural elements and assume values between 1 and 10 cm.

The truss-like bus structure is composed of 10 bays that are 3.0 m long by 1.5 m wide and high. Figure 10 indicates the connection of members to form a typical bay. The truss elements in the bus are tubes with a constant wall thickness of 0.159 cm and with outer radius controlled by design variable r_1 . The bays on each end of the bus include extra members to support the vibration suppression actuators located at the centers of these two bays. The actuators are modeled as point masses that are connected to each corner of the bay.

The flat, circular antennas with diameters of 15.0 and 7.5 m are formed with 12 radial and 12 circumferential beam elements. The antenna truss elements have the same wall thickness as the bus truss elements, but their outer radius is controlled by the design variable r_2 . The antennas are supported by truss members that connect the four joints on the top face of the last bay to the center of an antenna. The distance between the centerline of the bus structure and the plane of each antenna is 5 m. The outer radius of the antenna support members is controlled by r_3 .

The mass and inertia properties of the reference configuration and its static response characteristics are determined with EAL. Standard routines return the total mass, the truss structure mass, and the center-of-mass location. These routines also calculate the inertias about the center of mass. The partial derivatives of the truss mass and of the elements of the moment of inertia matrix with respect to r_i and M_{act} are approximated with a finite-difference technique.

The dynamic characteristics of the reference configuration are determined through solution of an eigenvalue problem of the form

$$\mathbf{K}\Psi - \omega^2\mathbf{M}\Psi = 0 \quad (\text{B1})$$

where \mathbf{K} is the stiffness matrix, \mathbf{M} is the mass matrix, ω^2 represent the eigenvalues, and Ψ represent the eigenvectors, normalized so that $\Psi_i^T \mathbf{M} \Psi_i$ equals unity.

Typical values of ω^2 are listed in table 1. The first 26 eigenvalues are listed for structures that correspond to three different cycles of demonstration case 1. The first six eigenvalues, which are associated with the rigid-body modes, are identically zero. Only the eigenvalues of the first 20 elastic modes are transmitted to the controls analysis. Also, the bold-face type in table 1 indicates the presence of repeated eigenvalues.

The partial derivatives of ω^2 and Ψ with respect to the design variables and the mass of actuators are calculated with semianalytic formulas described in references 18 and 19. For instance, the eigenvalue derivatives with respect to r_1 are given by

$$\frac{\partial(\omega^2)}{\partial r_1} = \Psi^T \left[\frac{\partial \mathbf{K}}{\partial r_1} - \omega^2 \frac{\partial \mathbf{M}}{\partial r_1} \right] \Psi \quad (\text{B2})$$

The derivatives of the stiffness and mass matrices can be accurately approximated with a finite-difference technique. Although the solution of the eigenvalue problem (eq. (B1)) is computationally expensive (e.g., 3 min of CPU time on a CONVEX 220 for the demonstration case), the partial derivatives of eigenvalues and eigenvectors can be calculated accurately and with little expense, especially if the mass and stiffness matrices are updated efficiently. (See ref. 19 for implementation details and cost estimates of various methods.)

When the solution to equation (B1) produces repeated eigenvalues, then the calculation of partial derivatives of those particular eigenvalues and of corresponding eigenvectors requires special care. (See ref. 22.) In the demonstration problem, repeated eigenvalues are caused by symmetry in the reference configuration. The mode shapes associated with repeated eigenvalues always involve bending or rotation of the antennas. Figure 11 shows the mode shapes for a typical pair of repeated eigenvalues. Since the bus structure is not involved in either mode, the rotational components of the matrix Ψ at the actuator locations must equal zero. Moreover, since the design variables do not influence the symmetry of the structure, the partial derivatives of these rotational

components with respect to structural parameters must also equal zero. Thus, the method developed in reference 22 is not required here.

The outputs of the structural analysis are M_s , \mathbf{J} , ω , and Ψ . The derivatives of these quantities with respect to M_{act} are calculated routinely, and the derivatives with respect to the structural design

variables are calculated once per cycle. The matrix Ψ contains modal displacements and rotations at each node in the finite-element model. Only the modal rotations that correspond to the three actuator locations are required by the controls analysis. Therefore, these rotations are extracted from the matrix Ψ and placed in matrices $\Phi^{(0)}$, $\Phi^{(1)}$, and $\Phi^{(2)}$.

Appendix C

Actuator Mass Calculation

The vibration suppression actuators, located at specified structural nodes, are sized so that they damp the elastic motion that results from a minimum-time reference rotational maneuver. To determine the actuator mass, a reduced-order model of the spacecraft, which is obtained by modal truncation, must first be provided to the control analysis from the structural analysis. Next, the vibration suppression control law must be defined. A closed-loop model results, which may be put into state-space form. The reference maneuver that excites the closed-loop system is next defined, and the response to this excitation is determined. The resulting vibration suppression torque histories are scanned to find peak values, and the required actuator mass is determined from these values. The remainder of this appendix describes the details of this procedure.

Eigenvalue analysis of a finite-element model of the spacecraft as described in appendix B allows construction of a truncated model in the control analysis. This reduced-order model consists of n elastic modes and has the general form

$$\ddot{\mathbf{q}} + \mathbf{D}\dot{\mathbf{q}} + \mathbf{\Lambda}\mathbf{q} = \mathbf{\Gamma}_t\mathbf{F} + \mathbf{\Gamma}_r\mathbf{T} \quad (\text{C1})$$

where \mathbf{q} represents an n -vector of unknown modal coordinates, $\ddot{\mathbf{q}}$ and $\dot{\mathbf{q}}$ are time derivatives, \mathbf{D} is a diagonal damping matrix with elements $2\rho\omega_i$, ρ is the modal damping ($\rho = 0.005$), $\mathbf{\Lambda}$ is a diagonal matrix of eigenvalues ω_i^2 , and $\mathbf{\Gamma}_t$ and $\mathbf{\Gamma}_r$ are translational and rotational components of the structural eigenvectors at the points where external forces \mathbf{F} and moments \mathbf{T} are applied. Reference 23 discusses the choice of an appropriate number of modes, and reference 24 discusses the classical transformation of the differential equations of motion from physical to modal coordinates. The explicit form of the right-hand side of this equation is determined once the vibration suppression system and the reference excitation are characterized.

The vibration suppression system employs a robust dissipative control strategy called collocated elastic control (CEC), since it provides stability despite unmodeled dynamics and parameter uncertainty. (See refs. 15 to 17.) Expressions for a single pair of CEC actuators that produce torques \mathbf{T}_1 and \mathbf{T}_2 (as in the demonstration problem) are developed here, although this procedure may be generalized to any number of actuators.

Collocated with the CEC torque actuators are attitude and attitude rate sensors. The actual attitude at each of the CEC actuator locations includes the rigid-body attitude \mathbf{a}_0 as well as the rotational elastic deformation. These angles are

$$\mathbf{a}_1 = \mathbf{a}_0 + \mathbf{\Phi}^{(1)}\mathbf{q} \quad \text{and} \quad \mathbf{a}_2 = \mathbf{a}_0 + \mathbf{\Phi}^{(2)}\mathbf{q} \quad (\text{C2})$$

Similarly the measured attitude rates are

$$\dot{\mathbf{a}}_1 = \dot{\mathbf{a}}_0 + \mathbf{\Phi}^{(1)}\dot{\mathbf{q}} \quad \text{and} \quad \dot{\mathbf{a}}_2 = \dot{\mathbf{a}}_0 + \mathbf{\Phi}^{(2)}\dot{\mathbf{q}} \quad (\text{C3})$$

To remove the effect of the rigid-body attitude and rate, the actuators act in a differential mode. Define

$$\left. \begin{aligned} \mathbf{a} &= \mathbf{a}_1 - \mathbf{a}_2 = \mathbf{\Phi}\mathbf{q} \\ \dot{\mathbf{a}} &= \dot{\mathbf{a}}_1 - \dot{\mathbf{a}}_2 = \mathbf{\Phi}\dot{\mathbf{q}} \end{aligned} \right\} \quad (\text{C4})$$

where $\mathbf{\Phi} = \mathbf{\Phi}^{(1)} - \mathbf{\Phi}^{(2)}$. The actuator outputs are constrained so that $\mathbf{T}_1 = -\mathbf{T}_2 \equiv \mathbf{W}$ so that the CEC system does not affect rigid-body motion. The control law has the form

$$\mathbf{W} = -\mathbf{G}_p\mathbf{a} - \mathbf{G}_r\dot{\mathbf{a}} \quad (\text{C5})$$

where the \mathbf{G}_p and \mathbf{G}_r are 3×3 positive-definite, symmetric position- and rate-gain matrices. Symmetry of the gain matrices is guaranteed implicitly by the following decompositions:

$$\mathbf{G}_p = \overline{\mathbf{G}}_p^T \overline{\mathbf{G}}_p \quad \text{and} \quad \mathbf{G}_r = \overline{\mathbf{G}}_r^T \overline{\mathbf{G}}_r \quad (\text{C6})$$

The 12 unique elements of the decomposed gain matrices $\overline{\mathbf{G}}_p$ and $\overline{\mathbf{G}}_r$ are the design variables \mathbf{g} . Thus,

$$\overline{\mathbf{G}}_p = \begin{bmatrix} g_1 & 0 & 0 \\ g_2 & g_3 & 0 \\ g_4 & g_5 & g_6 \end{bmatrix} \quad \text{and} \quad \overline{\mathbf{G}}_r = \begin{bmatrix} g_7 & 0 & 0 \\ g_8 & g_9 & 0 \\ g_{10} & g_{11} & g_{12} \end{bmatrix} \quad (\text{C7})$$

where $0 \leq g_i \leq 200$.

The closed-loop equations of motion are written with equation (C1). For now, the reference maneuver is given as some moment \mathbf{U} applied at a point. The closed-loop elastic equation of motion, which is obtained by considering both the reference maneuver and the CEC system, is

$$\ddot{\mathbf{q}} + \mathbf{D}\dot{\mathbf{q}} + \mathbf{\Lambda}\mathbf{q} = \mathbf{\Phi}^{(0)\text{T}}\mathbf{U} + \mathbf{\Phi}^{(1)\text{T}}\mathbf{T}_1 + \mathbf{\Phi}^{(2)\text{T}}\mathbf{T}_2 \quad (\text{C8})$$

where the $3 \times n$ mode-slope matrices $\mathbf{\Phi}^{(0)}$, $\mathbf{\Phi}^{(1)}$, and $\mathbf{\Phi}^{(2)}$ contain rotational components of the eigenvectors at the point of application of the maneuver moment \mathbf{U} and at the two CEC torque actuator locations. From $\mathbf{\Phi} = \mathbf{\Phi}^{(1)} - \mathbf{\Phi}^{(2)}$, equation (C8) can be written as

$$\ddot{\mathbf{q}} + \mathbf{D}\dot{\mathbf{q}} + \mathbf{\Lambda}\mathbf{q} = \mathbf{\Phi}^{(0)\text{T}}\mathbf{U} + \mathbf{\Phi}^T\mathbf{W} \quad (\text{C9})$$

By substitution for the control law (eq. (C5)) and use of equation (C4), the closed-loop equations of motion become

$$\ddot{\mathbf{q}} + \overline{\mathbf{D}}\dot{\mathbf{q}} + \overline{\mathbf{\Lambda}}\mathbf{q} = \mathbf{\Phi}^{(0)\text{T}}\mathbf{U} \quad (\text{C10})$$

where positive definite matrices $\overline{\mathbf{D}}$ and $\overline{\mathbf{\Lambda}}$ are

$$\left. \begin{aligned} \overline{\mathbf{D}} &= \mathbf{D} + \mathbf{\Phi}^T\mathbf{G}_r\mathbf{\Phi} \\ \overline{\mathbf{\Lambda}} &= \mathbf{\Lambda} + \mathbf{\Phi}^T\mathbf{G}_p\mathbf{\Phi} \end{aligned} \right\} \quad (\text{C11})$$

This system may easily be written in state-space form as

$$\dot{\mathbf{x}} = \mathbf{A}\mathbf{x} + \mathbf{B}\mathbf{U} \quad (\text{C12})$$

for the $2n$ states $\mathbf{x} = (\mathbf{q}^T, \dot{\mathbf{q}}^T)^T$. The $2n \times 2n$ matrix \mathbf{A} is

$$\mathbf{A} = \begin{bmatrix} \mathbf{0} & \mathbf{I} \\ -\overline{\mathbf{\Lambda}} & -\overline{\mathbf{D}} \end{bmatrix} \quad (\text{C13})$$

The $2n \times 3$ matrix \mathbf{B} is given by

$$\mathbf{B} = \begin{bmatrix} \mathbf{0} \\ \mathbf{\Phi}^{(0)\text{T}} \end{bmatrix} \quad (\text{C14})$$

The closed-loop eigenvalues, which are used as constraints in the optimization process, are the eigenvalues of matrix \mathbf{A} .

The response $\mathbf{x}(t)$ of the closed-loop system to a reference excitation dictates the required vibration suppression torques. This reference excitation was chosen to be a bang-bang type, minimum-time rotational maneuver given by

$$\mathbf{U}(t) = \begin{bmatrix} \mathbf{u}_1 \\ \mathbf{u}_2 \\ \mathbf{u}_3 \end{bmatrix} = \begin{cases} \mathbf{u}_{\max} & (0 \leq t < t_f/2) \\ -\mathbf{u}_{\max} & (t_f/2 \leq t < t_f) \\ 0 & (t \geq t_f) \end{cases} \quad (\text{C15})$$

where \mathbf{u}_{\max} is the maximum applied maneuver moment given by

$$\mathbf{u}_{\max} = \frac{4}{t_f^2}\mathbf{J}\boldsymbol{\alpha}_f \quad (\text{C16})$$

Here, u_i represents components of the maximum maneuver moment, t_f is the maneuver time, \mathbf{J} is the spacecraft inertia matrix, and $\boldsymbol{\alpha}_f$ is the vector of (small) desired attitude angles. (The reference excitation, which depends on \mathbf{J} , is different for each repetition of the controls analysis.) The initial orientation angles and times are assumed to be zero. Maneuver parameters t_f and $\boldsymbol{\alpha}_f$ remain fixed throughout the optimization procedure. The reference maneuver only exists to simulate a realistic disturbance to the spacecraft. Thus, the mass of the maneuver actuator (assumed to be zero) is never changed.

The actuator mass is determined by solving equation (C12) for the response $\mathbf{x}(t)$ and then calculating from equations (C4) and (C5) the actuator torque $\mathbf{W}(t)$, which is a function of \mathbf{x} . The response is given by

$$\mathbf{x}(t) = \exp(\mathbf{A}t)\mathbf{x}_0 + \exp(\mathbf{A}t) \int_0^t \exp(-\mathbf{A}\tau)\mathbf{B}\mathbf{U}(\tau) d\tau \quad (\text{C17})$$

Evaluating the convolution integral yields

$$\mathbf{x}(t) = \left\{ \begin{array}{ll} \mathbf{A}^{-1} [\exp(\mathbf{A}t) - \mathbf{I}] \mathbf{B}\mathbf{u}_{\max} & (0 \leq t \leq t_f/2) \\ \mathbf{A}^{-1} \{ \exp(\mathbf{A}t) - 2\exp[\mathbf{A}(t - t_f/2)] + \mathbf{I} \} \mathbf{B}\mathbf{u}_{\max} & (t_f/2 \leq t \leq t_f) \\ \mathbf{A}^{-1} \exp(\mathbf{A}t) [\exp(-\mathbf{A}t_f/2) - \mathbf{I}]^2 \mathbf{B}\mathbf{u}_{\max} & (t \geq t_f) \end{array} \right\} \quad (\text{C18})$$

This expression may be used to find the torque at any time by recalling that the CEC control law (eq. (C5)) may be rewritten as

$$\mathbf{W}(t) = [-\mathbf{G}_p \boldsymbol{\Phi} \quad | \quad -\mathbf{G}_r \boldsymbol{\Phi}] \mathbf{x}(t) \quad (\text{C19})$$

For the demonstration problem, the peak values of \mathbf{W} are found simply by scanning each required control torque history for each of the three coordinate directions for a sufficient period of time *after* the maneuver ends. Limiting the search to times greater than t_f allows calculation of the unforced response recursively at minimum computational cost (e.g., 10 sec of CPU time on the CONVEX 220). Thus,

$$\mathbf{x}_{i+1} = \exp(\mathbf{A} \Delta t)\mathbf{x}_i \quad (i = 0, 1, 2, \dots, n_t) \quad (\text{C20})$$

where $\mathbf{x}_0 = \mathbf{x}(t_f)$, and Δt is no greater than $P/2$, where P is the period of the highest vibration frequency in the truncated model, and n_t is the number of points scanned. For the demonstration cases, $\Delta t = P/16$ and the time histories are scanned starting at t_f for a time period equal to twice the period of the lowest vibration frequency.

Having identified the peak torques, the actuator mass is determined with a functional or empirical relationship between torque output and actuator mass. For the demonstration problem, a constant of proportionality is assumed, and the contributions to the total actuator mass from each coordinate direction are

$$(m_1, m_2, m_3)^T = 2M_T(w_1^*, w_2^*, w_3^*)^T = 2M_T\mathbf{W}^* \quad (\text{C21})$$

where $w_i^* = |w_i(t_i^*)|$ is the peak torque occurring at time t_i^* for the i th coordinate direction, and M_T is the constant of proportionality between mass and torque output ($M_T = 1.0 \text{ lbf}/\text{ft-lbf} = 0.334 \text{ kg}/\text{N-m}$). The factor of 2 exists because there are two CEC actuators. The actuator mass then is

$$M_{\text{act}} = m_1 + m_2 + m_3 \quad (\text{C22})$$

Appendix D

Computer Implementation

The integrated controls-structures optimization procedure is implemented as a batch job on a CONVEX 220 computer. The procedure consists of a set of FORTRAN codes that are linked by operating system commands and by input and output (I/O) files. The operating system on the CONVEX computer is a derivative of UNIX, and the command language interpreter is similar to the C shell (csh) available on many machines. Table 2 contains a list of all FORTRAN codes and their I/O files.

The batch job developed for the current research is useful as a model of a generic optimization procedure for coupled, multidisciplinary optimization problems. This batch job can be modified to address a variety of controls-structures integrated design (CSID) optimization problems. Figure 12 is a list of the batch submittal file, and figure 13 is a conceptual flowchart that explains the operation of the batch job. In figure 13, the rectangles represent FORTRAN programs, the diamonds represent logical tests, the heavy lines indicate normal data flow, and the dashed lines indicate a shortcut, which is used whenever possible. The numbers in parentheses beside the flowchart correspond to numbered comments in figure 12.

The command language implementation scheme has a number of advantages over the traditional programming language (e.g., FORTRAN) implementation. This is a time-consuming procedure (e.g.,

one demonstration problem required about 25 hr of CPU time on the CONVEX computer). This command language implementation facilitates monitoring, restarting, and debugging the process. Since each execution of each FORTRAN program creates new output files, a simple list of file names and times of creation is used to deduce the state of an executing process. At the same time, any output file can be examined or printed to obtain information about the progress of the optimization. If the optimizer or analysis routines do not appear to be operating correctly, the process can be stopped and restarted at the current step or at a previous step. To restart at the beginning of any cycle, only the files "VARIABLE," "M.act," and "history.old" need to be edited to contain the design point, the initial estimate of actuator mass, and the history of previous optimization cycles. If the process stops abnormally, then files such as the Engineers Analysis Language (EAL) input and output files, which normally are not printed, are examined for the cause of the failure.

A final advantage of this command language implementation is computer resource management. As each FORTRAN execution is completed, the batch job condenses the output and deletes as many files as possible. Thus, complete information is available for debugging when the process stops abnormally, but the disk space is saved when the process executes normally. The filtering tools available in a UNIX-based operating environment (e.g., "grep") are used to extract a summary of information in each output file before the file is deleted. (See fig. 12.)

References

1. Newsom, Jerry R.; Layman, W. E.; Waites, H. B.; and Hayduk, R. J.: *The NASA Controls-Structures Interaction Technology Program*. NASA TM-102752, 1990.
2. Newsom, Jerry R., compiler: *NASA/DOD Controls-Structures Interaction Technology 1989*. NASA CP-3041, 1989.
3. *A Collection of Technical Papers AIAA Dynamics Specialist Conference*. CP-903, American Inst. of Aeronautics and Astronautics, Inc., Apr. 1990.
4. Haftka, Raphael T.: Integrated Structure-Control Optimization of Space Structures. *A Collection of Technical Papers AIAA Dynamics Specialist Conference*, CP-903, American Inst. of Aeronautics and Astronautics, Inc., Apr. 1990, pp. 1-9. (Available as AIAA-90-1190-CP.)
5. Belvin, W. Keith; Edighoffer, Harold H.; and Herstrom, Catherine L.: Quasistatic Shape Adjustment of a 15-Meter-Diameter Space Antenna. *J. Spacecr. & Rockets*, vol. 26, no. 3, May-June 1989, pp. 129-136.
6. Padula, Sharon L.; Sandridge, Chris A.; Walsh, Joanne L.; and Haftka, Raphael T.: Integrated Controls-Structures Optimization of a Large Space Structure. *A Collection of Technical Papers, Part 1 AIAA/ASME/ASCE/AHS/ASC 31st Structures, Structural Dynamics and Materials Conference*, American Inst. of Aeronautics and Astronautics, Apr. 1990, pp. 258-267. (Available as AIAA-90-1058-CP.)
7. Maghami, P. G.; Walz, J. E.; Joshi, S. M.; and Armstrong, E. S.: Integrated Controls-Structures Design Methodology Development for a Class of Flexible Spacecraft. *Third Air Force/NASA Symposium on Recent Advances in Multidisciplinary Analysis and Optimization - A Collection of Technical Papers*, Sept. 1990, pp. 1-6.
8. Belvin, Wendell Keith: *Simulation and Interdisciplinary Design Methodology for Control-Structure Interaction Systems*. Ph.D. Diss., Univ. of Colorado, 1989.
9. Sparks, Dean W., Jr.; Horner, Garnett C.; Juang, Jer-Nan; and Klose, Gerhard: *A Survey of Experiments and Experimental Facilities for Active Control of Flexible Structures*. NASA/DOD Controls-Structures Interaction Technology 1989, Jerry R. Newsom, compiler, NASA CP-3041, 1989, pp. 285-315.
10. Sobieszczanski-Sobieski, J.: Sensitivity of Complex, Internally Coupled Systems. *AIAA J.*, vol. 28, no. 1, Jan. 1990, pp. 153-160.
11. Levine, M.; Ide, H.; and Hollowell, S.: Multidisciplinary Hypersonic Configuration Optimization. *Third Air Force/NASA Symposium on Recent Advances in Multidisciplinary Analysis and Optimization - A Collection of Technical Papers*, Sept. 1990, pp. 412-417.
12. Barthelemy, J.-F. M.; Coen, P. G.; Wrenn, G. A.; Riley, M. F.; Dovi, A. R.; and Hall, L. E.: *Application of Multidisciplinary Optimization Methods to the Design of a Supersonic Transport*. NASA TM-104073, 1991.
13. James, Benjamin B.: An Alternative Formulation of the Global Sensitivity Equations. *Third Air Force/NASA Symposium on Recent Advances in Multidisciplinary Analysis and Optimization - A Collection of Technical Papers*, Sept. 1990, pp. 601-606.
14. Whetstone, W. D.: *EISI-EAL Engineering Analysis Language Reference Manual - EISI-EAL System Level 2091, Volume 1: General Rules and Utility Processors*. Engineering Information Systems, Inc., July 1983.
15. Joshi, S. M.: Robustness Properties of Collocated Controllers for Flexible Spacecraft. *J. Guid., Control, & Dyn.*, vol. 9, no. 1, Jan.-Feb. 1986, pp. 85-91.
16. Benhabib, R. J.; Iwens, R. P.; and Jackson, R. L.: Stability of Large Space Structure Control Systems Using Positivity Concepts. *J. Guid. & Control*, vol. 4, no. 5, Sept.-Oct. 1981, pp. 487-494.
17. Joshi, S. M.: *A Controller Design Approach for Large Flexible Space Structures*. NASA CR-165717, 1981.
18. Haftka, R. T.; and Adelman, H. M.: Recent Developments in Structural Sensitivity Analysis. *Struct. Optim.*, vol. 1, no. 3, Sept. 1989, pp. 137-151.
19. Sutter, Thomas R.; Camarda, Charles J.; Walsh, Joanne L.; and Adelman, Howard M.: Comparison of Several Methods for Calculating Vibration Mode Shape Derivatives. *AIAA J.*, vol. 26, no. 12, Dec. 1988, pp. 1506-1511.
20. Hajela, P.; Bloebaum, C. L.; and Sobieszczanski-Sobieski, J.: Application of Global Sensitivity Equations in Multidisciplinary Aircraft Synthesis. *J. Aircr.*, vol. 27, no. 12, Dec. 1990, pp. 1002-1010.
21. Vanderplaats, Garret N.: *CONMIN - A FORTRAN Program for Constrained Function Minimization, User's Manual*. NASA TM X-62282, 1973.
22. Mills-Curran, William C.: Calculation of Eigenvector Derivatives for Structures With Repeated Eigenvalues. *AIAA J.*, vol. 26, no. 7, July 1988, pp. 867-871.
23. Woodard, Stanley E.; Padula, Sharon L.; Graves, Philip C.; and James, Benjamin B.: An Optimization Method for Controlled Space Structures With Variable Actuator Mass. *Proceedings of the Fourth NASA/DOD Control/Structures Interaction Technology Conference*, Andrew D. Swanson, compiler, WL-TR-91-3013, U.S. Air Force, Jan. 1991, pp. 411-428.
24. Hurty, Walter C.; and Rubinstein, Moshe F.: *Dynamics of Structures*. Prentice-Hall, Inc., c.1964.

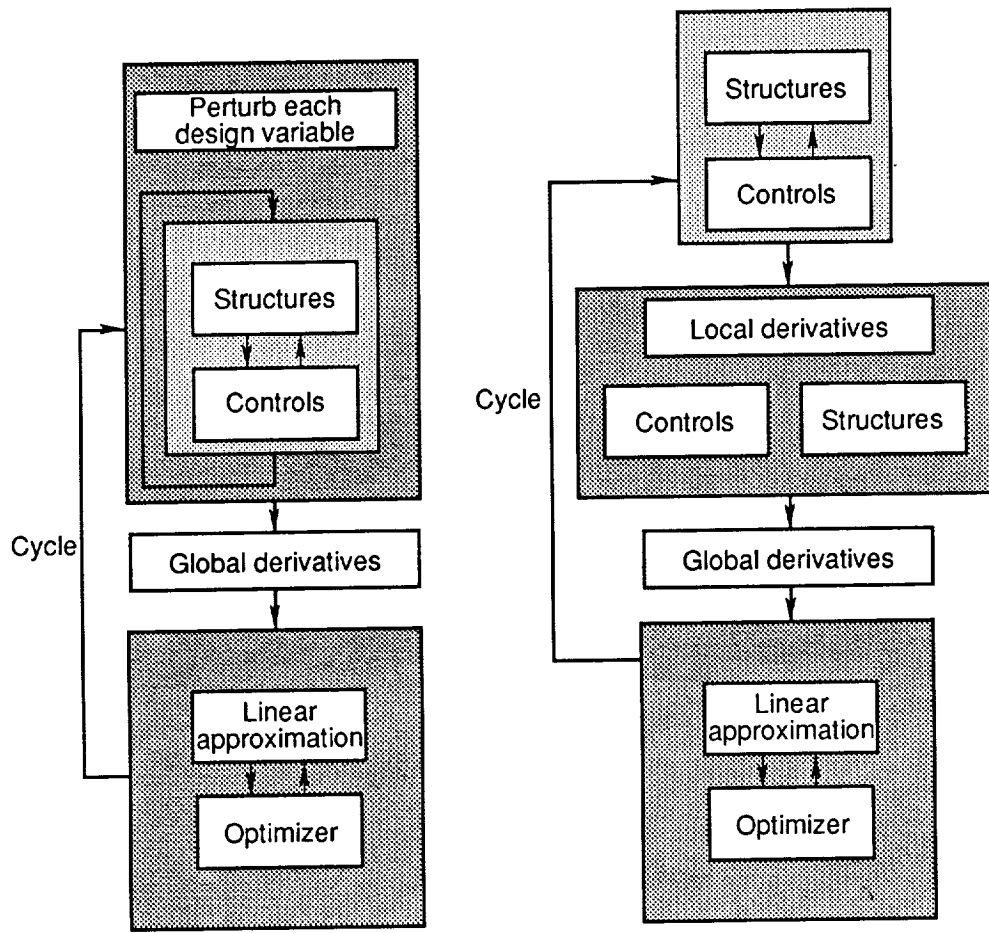
Table 1. Eigenvalues Calculated During Optimization Cycle
in Demonstration Case 1

[These cycles represent the initial and final conditions
and one intermediate result; bold-face type indicates
repeated eigenvalues]

Mode no.	Eigenvalues for—		
	Cycle 0	Cycle 6	Cycle 27
1	0	0	0
2	0	0	0
3	0	0	0
4	0	0	0
5	0	0	0
6	0	0	0
7	17.6	34.0	18.2
8	37.7	123.1	36.6
9	71.5	195.9	75.5
10	86.7	272.9	85.1
11	86.7	310.4	85.1
12	89.0	310.4	101.8
13	156.8	333.6	159.4
14	407.5	661.3	325.6
15	407.5	1524.0	399.1
16	442.0	1531.0	399.1
17	530.1	1531.0	506.1
18	787.6	1914.0	821.0
19	1114.0	2797.0	1114.0
20	1350.0	4954.0	1320.0
21	1350.0	4954.0	1320.0
22	1387.0	5216.0	1360.0
23	1387.0	5264.0	1360.0
24	2588.0	5264.0	1871.0
25	2588.0	6733.0	2061.0
26	2600.0	9102.0	2531.0

Table 2. FORTRAN Programs With Corresponding Input and Output Files Used by CSID Procedure

Program name	Input files	Output files
precal	M.act, modes.old, VARIABLE, eal.old	modes.dat, eal.in
EAL version 324	eal.in	eal.out
postcal	eal.out	modes.dat, gse.dat
MACT	modes.dat, actcon.dat, VARIABLE	actmass.out, M.act
dMACT	modes.dat, actcon.dat history.old, VARIABLE	history.new, cderv.dat
gseblld	gse.dat, cderv.dat, actcon.dat, VARIABLE modes.dat	DESVARBL
optimz	DESVARBL, FIXEDPAR history.new	VARIABLE, M.act



(a) Conventional CSID procedure. (b) Alternate CSID procedure that uses global sensitivity equations.

Figure 1. Optimization approaches for coupled controls-structures integrated design (CSID) problems.

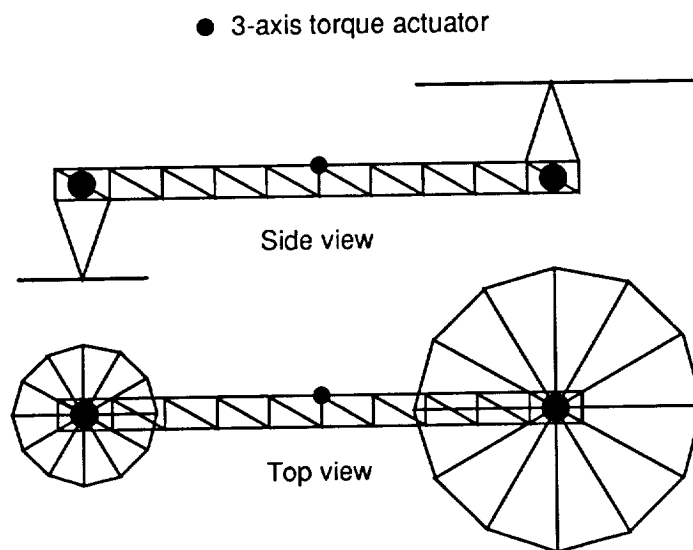


Figure 2. Reference configuration of geostationary platform with three-axis torque actuators.

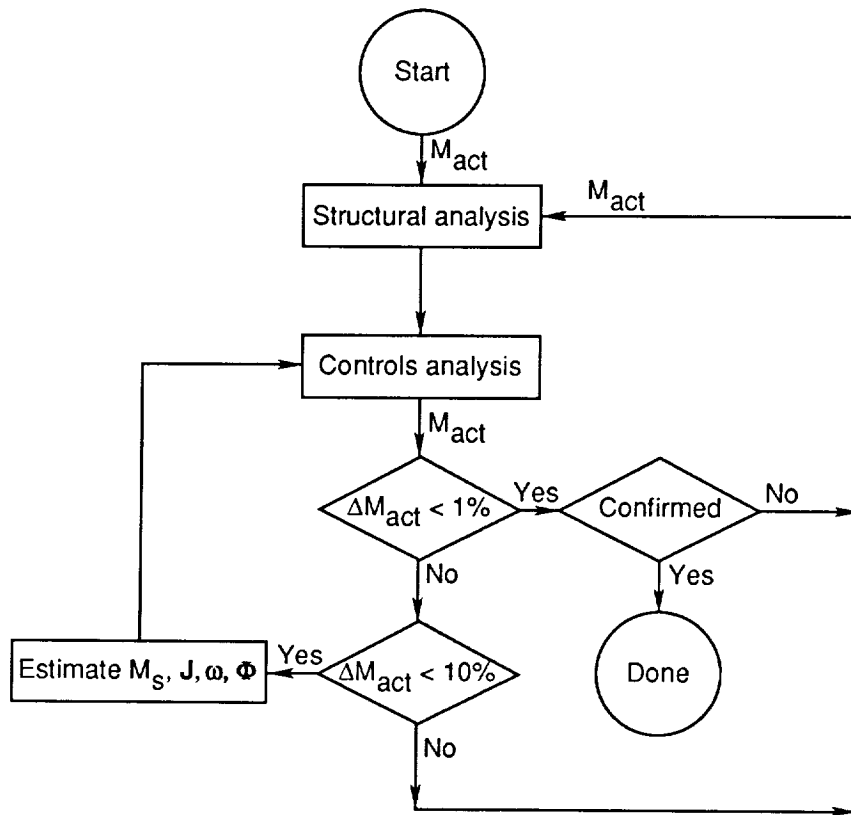


Figure 3. Flowchart of iterative procedure for coupled analysis.

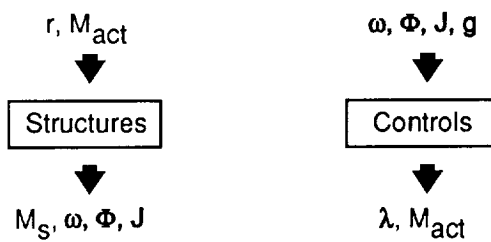
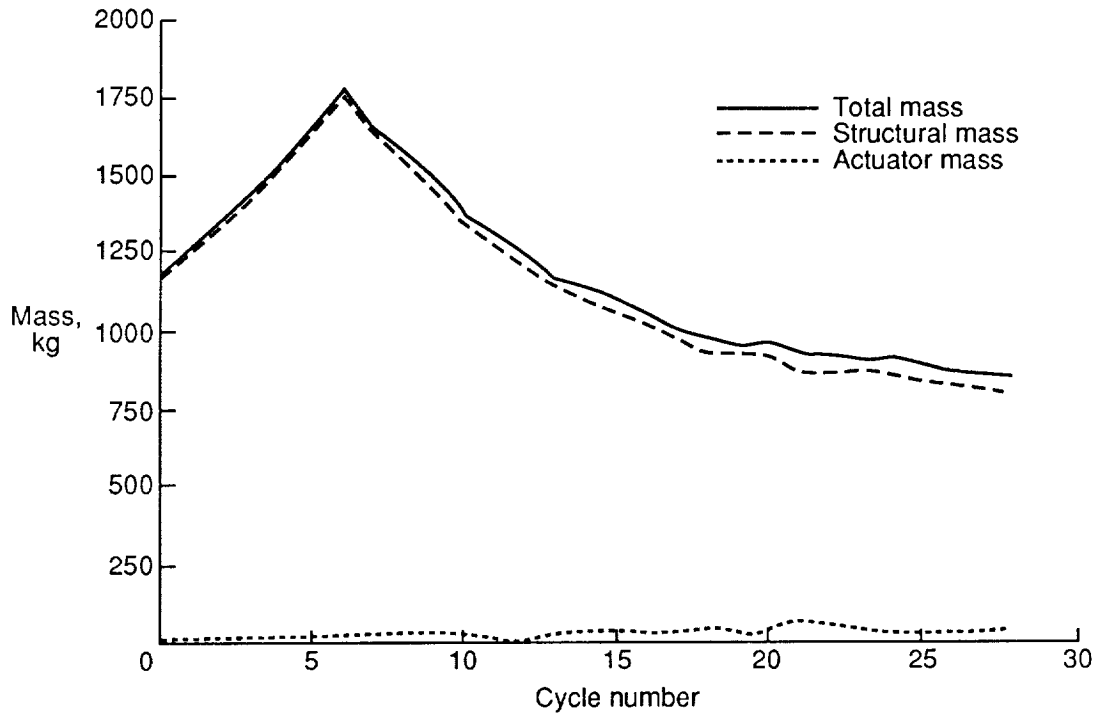
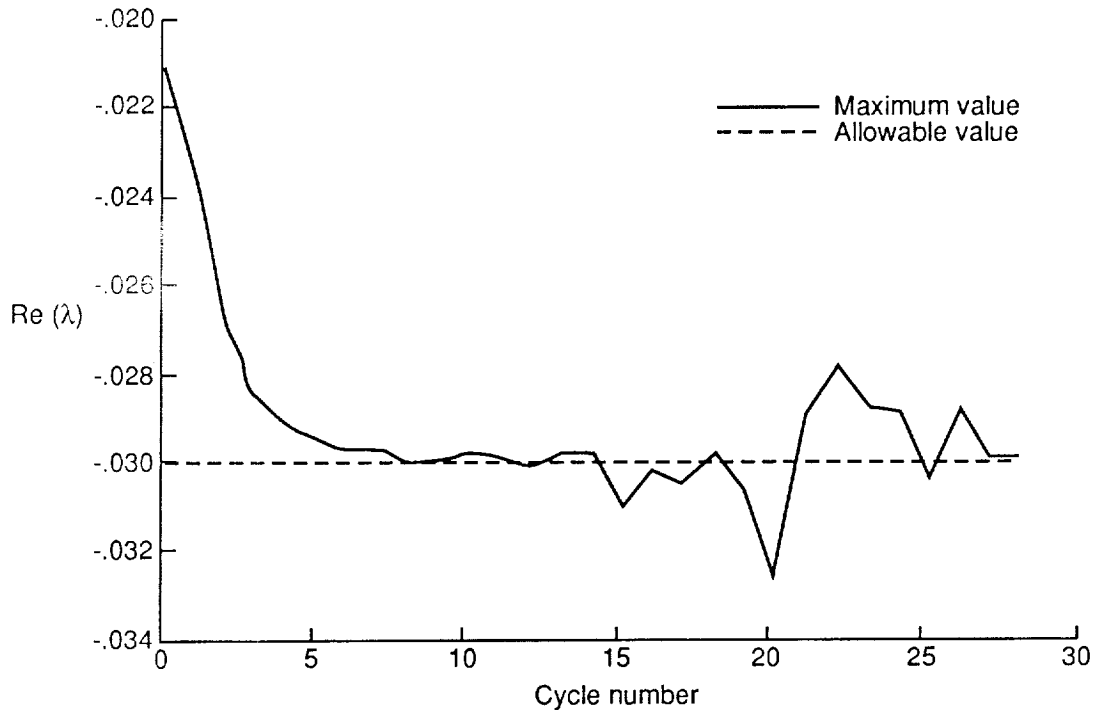


Figure 4. Input and output quantities for contributing analyses.

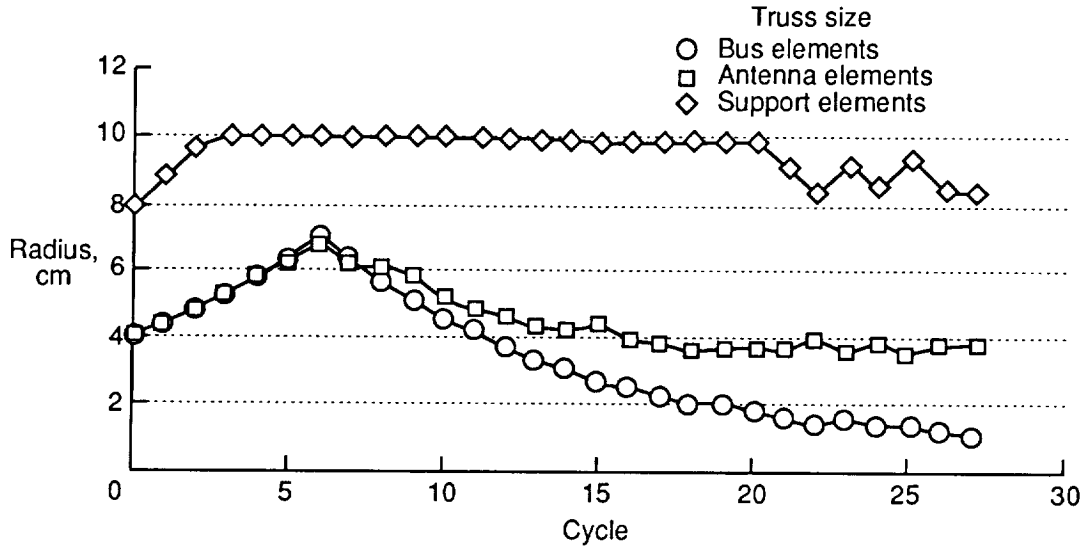


(a) Optimization history of mass of actuators, structure, and total geostationary platform.

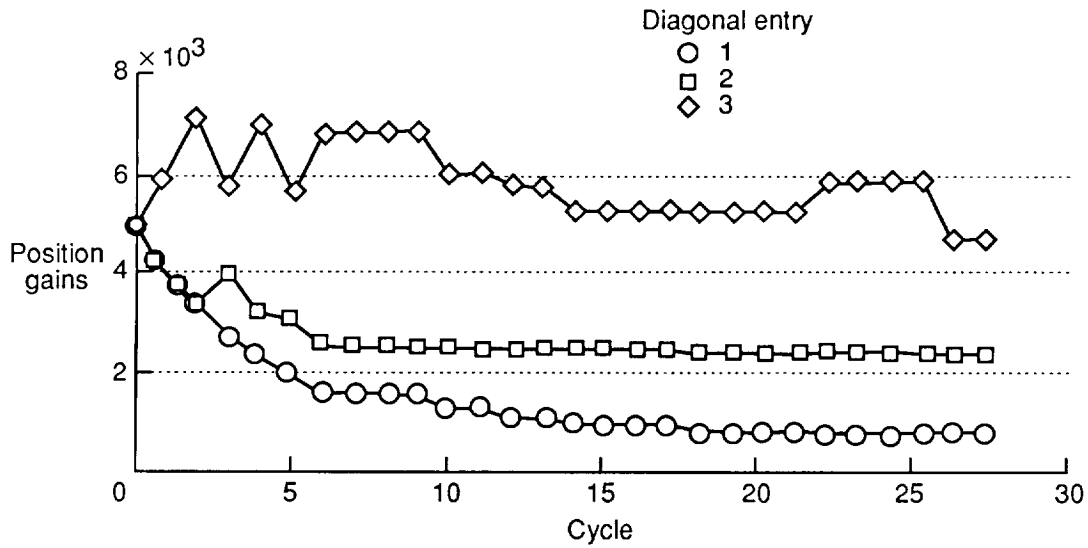


(b) Optimization history of maximum closed-loop eigenvalue compared to its allowable value. Constraint is initially violated.

Figure 5. Results of demonstration case 1.

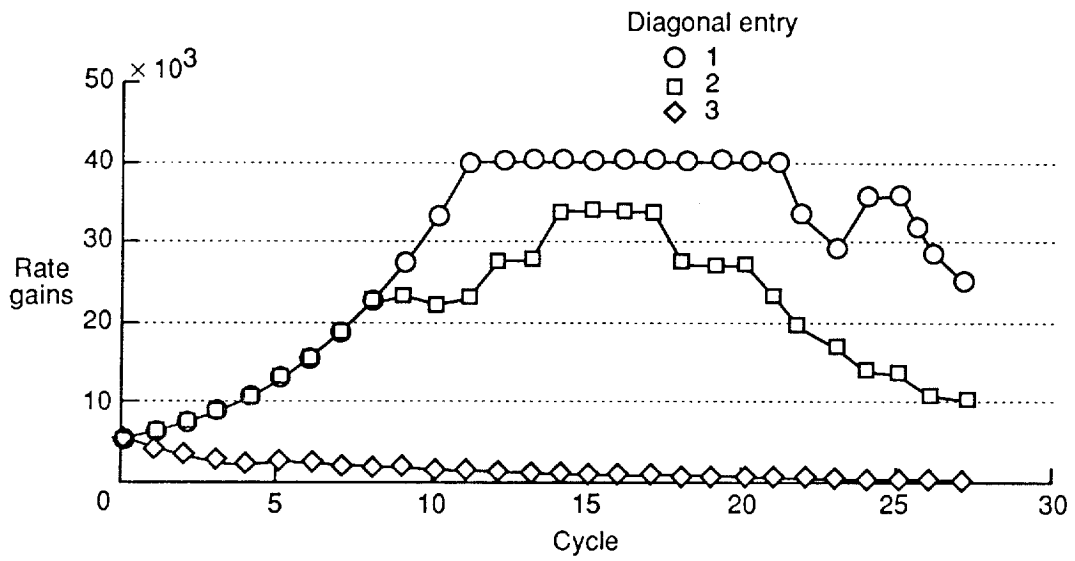


(c) Optimization history of structural design variable values.

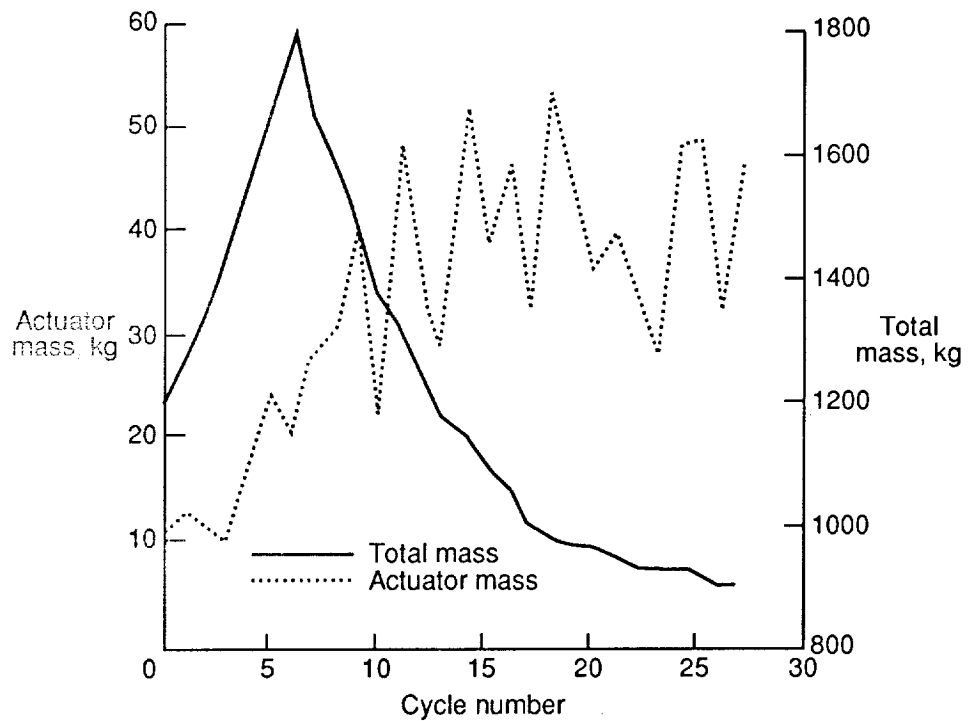


(d) Optimization history of position-gain matrix values. Diagonal elements of \mathbf{G}_p are shown.

Figure 5. Continued.



(c) Optimization history of rate-gain matrix values. Diagonal elements of \mathbf{G}_r are shown.



(f) Optimization history for mass of actuators and total mass.

Figure 5. Concluded.

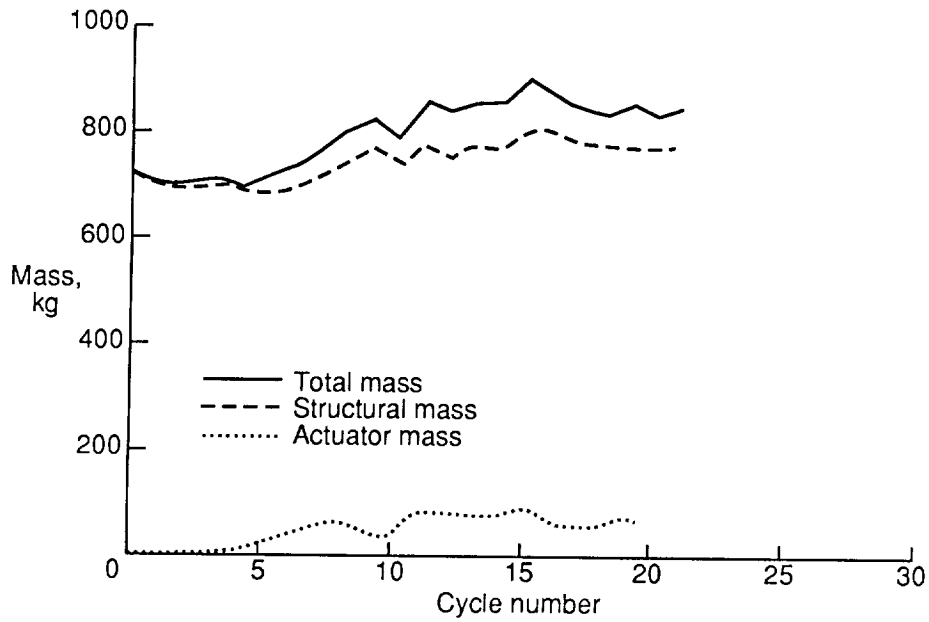


Figure 6. Optimization history of mass with respect to optimization cycle in demonstration case 2.

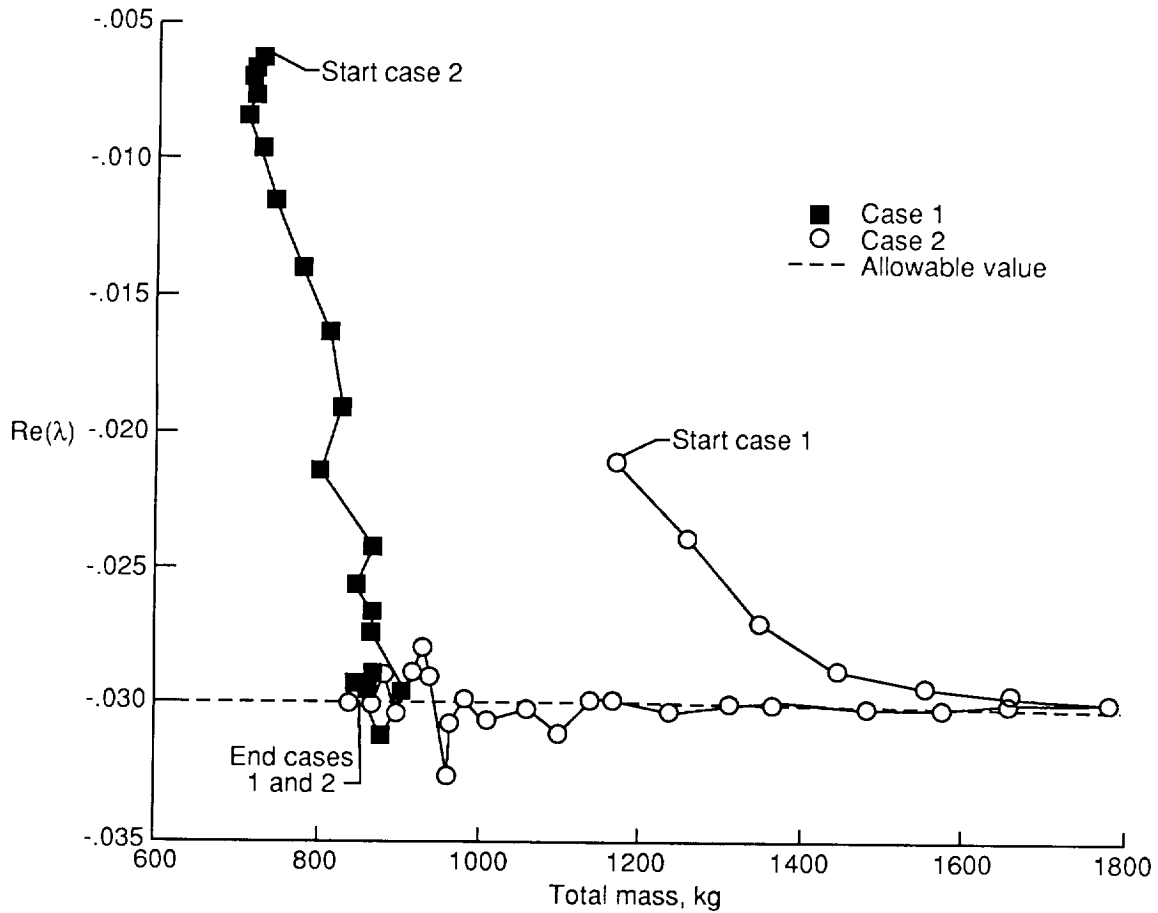
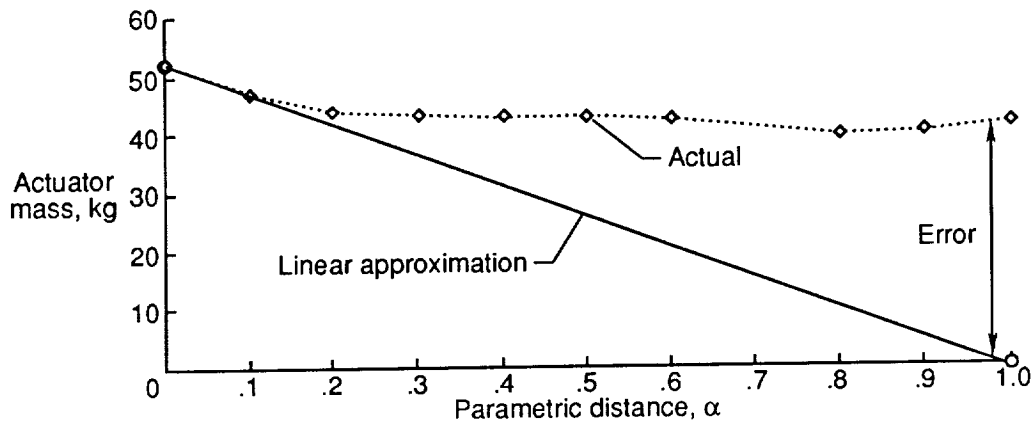
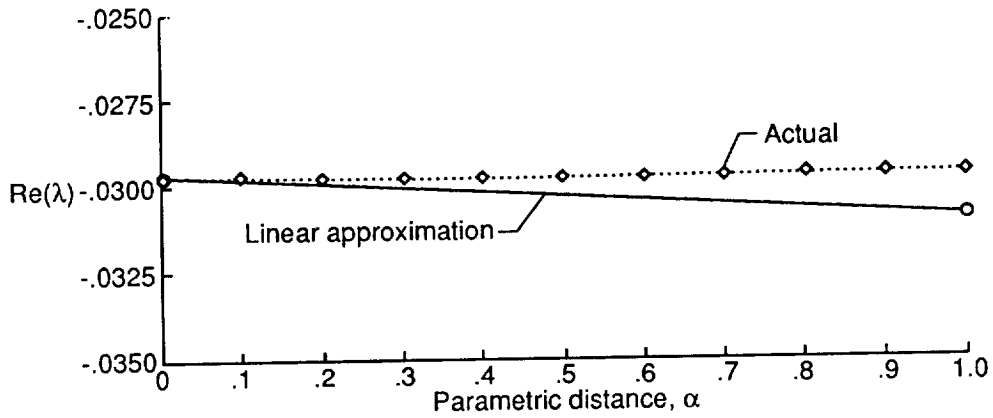


Figure 7. Comparison of optimization histories of demonstration cases 1 and 2. These cases start from different points in design space and converge to equivalent designs.



(a) Mass of actuators.



(b) Real part of maximum closed-loop eigenvalue.

Figure 8. Comparison of actual computed values of selected outputs of coupled controls-structures analysis with linear approximation to those values.

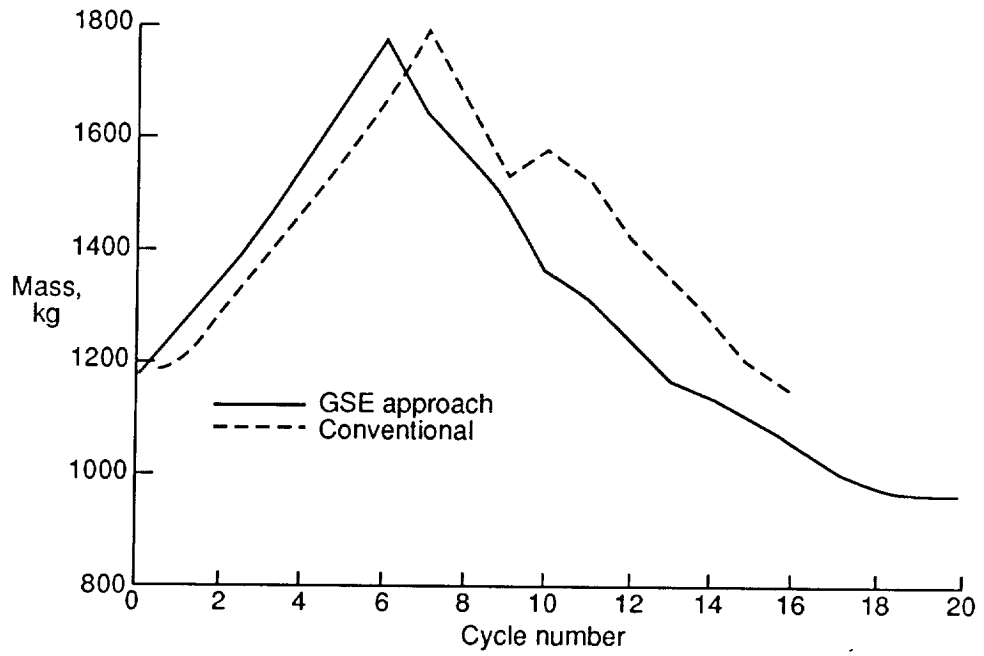


Figure 9. Comparison of optimization histories of demonstration case 1 with GSE and conventional approaches.

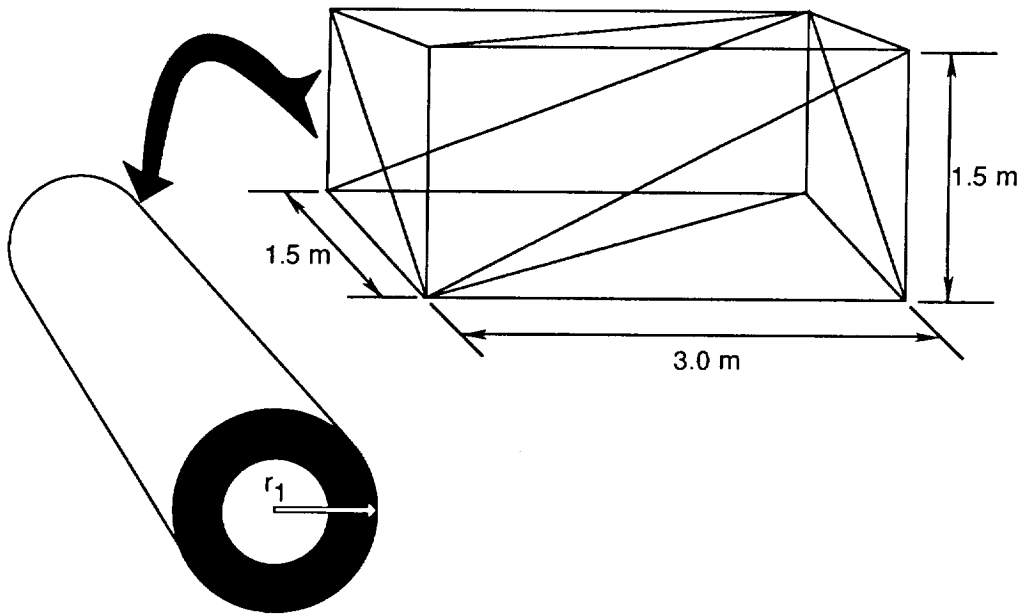


Figure 10. Typical bay of truss structure for reference configuration.

● Actuator locations

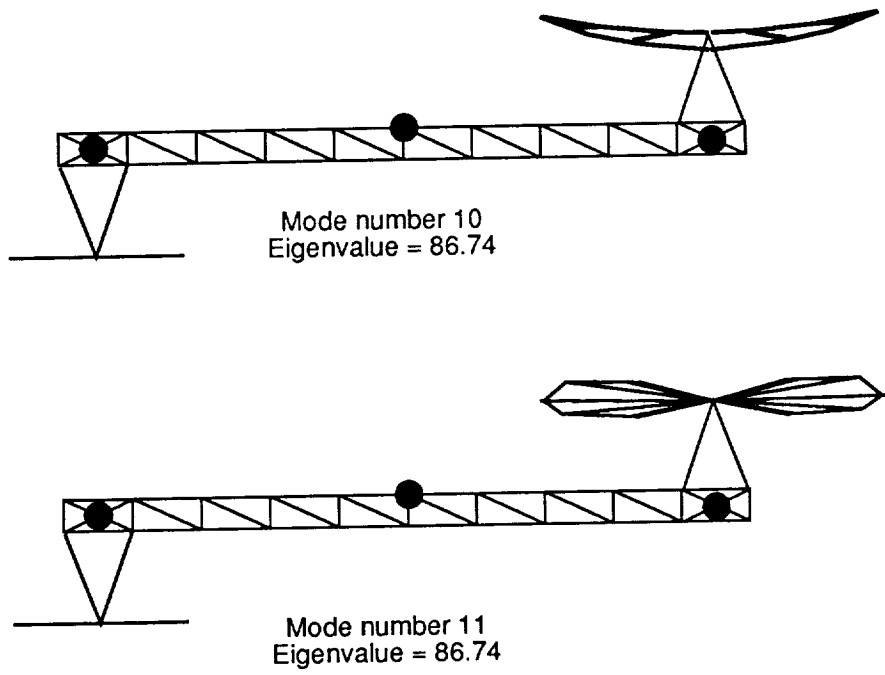


Figure 11. Typical mode shapes for eigenvectors of repeated eigenvalues.

```

#!/bin/csh
#@$-o output -eo -nr
#
#   INITIALIZATION
#
#   copy input files to scratch disk
#
date
if ( -f actcon.dat ) then
  echo RESTART   do not copy anything
else
  echo copy all files needed for optimization
  cp ~/eal.new eal.old
  cp ~/M.act M.act
  cp ~/VARIABLE VARIABLE
  cp ~/FIXEDPAR FIXEDPAR
  cp ~/history.old history.old
  cp ~/preeal preeal
  cp ~/posteal posteal
  cp ~/MACT MACT
  cp ~/dMACT dMACT
  cp ~/gsebld gsebld
  cp ~/optimz optimz
  cp ~/actcon.dat actcon.dat
endif
rm L*
rm modes.dat
@ numopt = 0
#
# (9)  new cycle?
#   Repeat the outer loop as long as a file "VARIABLE" exists
#
while ( -e VARIABLE )
#
#   reset counters
#
  rm DESVARBL
  @ cycle = 0
  @ ealcnt = 0
  @ macnt = 0
#
# (5)  converged?
#
#   Iterate between EAL and MACT until new mass of actuator
#   and previous mass of actuator are close enough
#   Repeat inner loop as long as file "M.act" exists

```

Figure 12. Batch submittal file for implementation of CSID procedure with UNIX command language.

```

#
# note: inner loop terminates abnormally after 7 calls to EAL
#       or after 50 approximations to EAL output
#
while ( -e M.act )
  @ cycle++
  echo CYCLE $cycle
  if ( $ealcnt >= 7 ) then
    echo MACT output
    cat actmass.out
    exit 1
  endif
  if ( $macnt >= 50 ) then
    echo actmass output
    cat actmass.out
    exit 1
  endif
endif
#
# (1)   EAL PREPROCESSOR
#
preeal
echo preeal completed
mv M.act mass.act
#
if ( -e modes.dat ) then
#
# ACTUATOR MASS CALCULATION
# use estimated frequencies
#
  @ macnt++
  echo start MACT   approximate analysis $macnt
  MACT
  echo MACT completed
  grep "mass" actmass.out
  mv modes.dat modes.old
else
#
# (2)   EAL Structural Analysis
# calculate actual frequencies
#
  @ ealcnt++
  echo start EAL   full analysis $ealcnt
  ~eal/eal324/eal324 <eal.in >eal.out
  echo EAL completed
  rm L*

```

Figure 12. Continued.

```

#
# (3)      POSTPROCESSOR
#
      cat eal.out|grep -v DATA|grep -v EX    >eal.log
      echo Prepare input to actmass
      posteal
      echo posteal completed
#
# (4)      ACTUATOR MASS CALCULATION
#
      echo Calculate actuator mass
      MACT
      echo MACT completed
      grep "mass" actmass.out
      mv modes.dat modes.old
    endif
  end
  echo converged
  echo DESIGN VARIABLES
  cat VARIABLE
  echo Structures model
  grep " J=" eal.in
  echo Structures output
  cat modes.old
#
# (5)      END INNER LOOP
#
  echo
#
# (6)      dMACT needs modes.dat to estimate f.d. derivatives
#
  cp modes.old modes.dat
  dMACT
  echo Controls output
  cat actmass.out
  echo dMACT completed
#
# (7)      gsebld assembles and solves GSE
#
  echo output from gsebld
  gsebld
  echo gsebld completed

```

Figure 12. Continued.

```

#
# (8) Global derivatives are in a file named "DESVARBL"
#     This file not produced if design is feasible and objective
#     stops improving
#
#     @ numopt++
#     echo BEGIN OPTIMIZATION $numopt
#     if ( -e DESVARBL ) then
#         cat DESVARBL
#         rm VARIABLE
#     else
#         exit 1
#     endif
#
# (9) check maximum number of optimization cycles
#
#     if ( $numopt >= 10 ) then
#         optimz
#         echo FINAL CYCLE optimz completed
#         echo output from optimz
#         cat OPTRESLT
#         echo HISTORY of OPTIMIZATION
#         cat history.new
#         mv history.new history.old
#         echo completed
#         exit 1
#     else
#         optimz
#         mv history.new history.old
#         echo optimz completed
#         echo output from optimz
#         cat OPTRESLT
#
#     endif
#
# if modes.dat exists - the inner loop will skip EAL
# rm modes.dat
#
# date
# end
#     END OUTER LOOP
#
#

```

Figure 12. Concluded.

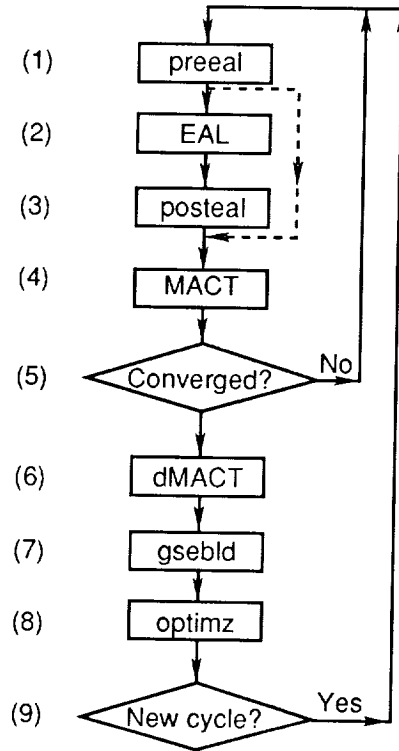


Figure 13. Flowchart of CSID procedure with GSE approach. See table 2 for FORTRAN programs and figure 12 for numbered comments.

INTERIMINARY PLANS

REPORT DOCUMENTATION PAGE			Form Approved OMB No. 0704-0188	
Public reporting burden for this collection of information is estimated to average 1 hour per response, including the time for reviewing instructions, searching existing data sources, gathering and maintaining the data needed, and completing and reviewing the collection of information. Send comments regarding this burden estimate or any other aspect of this collection of information, including suggestions for reducing this burden, to Washington Headquarters Services, Directorate for Information Operations and Reports, 1215 Jefferson Davis Highway, Suite 1204, Arlington, VA 22202-4302, and to the Office of Management and Budget, Paperwork Reduction Project (0704-0188), Washington, DC 20503.				
1. AGENCY USE ONLY (Leave blank)	2. REPORT DATE November 1991	3. REPORT TYPE AND DATES COVERED Technical Paper		
4. TITLE AND SUBTITLE Multidisciplinary Optimization of Controlled Space Structures With Global Sensitivity Equations			5. FUNDING NUMBERS WU 506-43-41-01	
6. AUTHOR(S) Sharon L. Padula, Benjamin B. James, Philip C. Graves, and Stanley E. Woodard				
7. PERFORMING ORGANIZATION NAME(S) AND ADDRESS(ES) NASA Langley Research Center Hampton, VA 23665-5225			8. PERFORMING ORGANIZATION REPORT NUMBER	
9. SPONSORING/MONITORING AGENCY NAME(S) AND ADDRESS(ES) National Aeronautics and Space Administration Washington, DC 20546-0001			10. SPONSORING/MONITORING AGENCY REPORT NUMBER NASA TP-3130	
11. SUPPLEMENTARY NOTES Padula and Woodard: Langley Research Center, Hampton, VA; James: Lockheed Engineering & Sciences Company, Hampton, VA; Graves: ViGYAN, Inc., Hampton, VA.				
12a. DISTRIBUTION/AVAILABILITY STATEMENT Unclassified-Unlimited Subject Category 18			12b. DISTRIBUTION CODE	
13. ABSTRACT (Maximum 200 words) A new method for the preliminary design of controlled space structures is presented. The method coordinates standard finite-element structural analysis, multivariable controls, and nonlinear programming codes and allows simultaneous optimization of the structures and control systems of a spacecraft. Global sensitivity equations are a key feature of this method. The preliminary design of a generic geostationary platform is used to demonstrate the multidisciplinary optimization method. Fifteen design variables are used to optimize truss-member sizes and feedback-gain values. The goal is to reduce the total mass of the structure and the vibration control system while satisfying constraints on vibration decay rate. Incorporating the nonnegligible mass of actuators causes an essential coupling between structural design variables and control design variables. The solution of the demonstration problem is an important step toward a comprehensive preliminary design capability for structures and control systems. Use of global sensitivity equations helps solve optimization problems that have a large number of design variables and a high degree of coupling between disciplines.				
14. SUBJECT TERMS Optimization; Spacecraft control; Large space structures; Spacecraft design			15. NUMBER OF PAGES 36	
			16. PRICE CODE A03	
17. SECURITY CLASSIFICATION OF REPORT Unclassified	18. SECURITY CLASSIFICATION OF THIS PAGE Unclassified	19. SECURITY CLASSIFICATION OF ABSTRACT	20. LIMITATION OF ABSTRACT	

NSN 7540-01-280-5500

Standard Form 298 (Rev. 2-89)
Prescribed by ANSI Std. Z39-18
298-102

NASA-Langley, 1991

PRECEDING PAGE BLANK NOT FILMED

~~SECRET~~